# *TSC2* loss in neural progenitor cells suppresses translation of ASD/NDD-associated transcripts in an mTORC1- and MNK1/2-reversible fashion

Pauline Martin,[1, 4] Krzysztof J. Szkop,[2, 4] Francis Robert,[3, 4] Srirupa Bhattacharyya,[1] Roberta L. Beauchamp,[1] Jacob Brenner, [1] Nicholas E. Redmond[1], Sidong Huang,[3] Serkan Erdin,[1] Ola Larsson,[2*] Vijaya Ramesh[1*§]

[1]Center for Genomic Medicine, Department of Neurology, Massachusetts General Hospital, Boston, MA 02114, USA; [2]Department of Oncology-Pathology, Science for Life Laboratory, Karolinska Institute, Stockholm 171 77, Sweden; [3]Department of Biochemistry and Goodman Cancer Research Institute, McGill University, Montreal, PQ H3G1Y6, Canada; [4]These authors contributed equally to this work.

* Co-corresponding senior authors: Ola Larsson (ola.larsson@ki.se), Vijaya Ramesh (ramesh@helix.mgh.harvard.edu)

§ **Lead contact:** Vijaya Ramesh, 185 Cambridge Street, Boston, MA 02114. Phone: 617-724-9733; Email: ramesh@helix.mgh.harvard.edu

## SUMMARY

Tuberous sclerosis complex (TSC), an inherited neurodevelopmental (ND) disorder with frequent manifestations of epilepsy and autism spectrum disorder (ASD). TSC is caused by mutations in *TSC1* or *TSC2* tumor suppressor genes, with encoded proteins hamartin/TSC1 and tuberin/TSC2 forming a functional complex inhibiting mechanistic target of rapamycin complex-1 (mTORC1) signaling, leading to FDA-approved allosteric mTORC1-selective rapamycin analogs for TSC tumors. Rapalogs are effective for TSC-associated hamartomas, however, they are not effective for treating ND manifestations. mTORC1 signaling plays an essential role in protein synthesis through mTORC1-eIF4F and MNK-eIF4E-mediated mRNA translation. Further, the effects on mRNA translation by specific mTORC1 and MNK inhibitors such as RMC-6272 and eFT-508 in TSC have never been explored. Here, employing CRISPR-modified, isogenic TSC2 patient-derived neural progenitor cells (NPCs), we have examined mRNA translation upon loss of *TSC2*. Our results reveal dysregulated translation in *TSC2*-Null NPCs, which significantly overlap with the translatome from *TSC1*-Null NPCs, which we reported recently. Most notably, numerous non-monogenic ASD- NDD- and epilepsy-associated genes identified in patients harboring putative loss-of-function mutations, including protein truncating, or damaging missense variants, were translationally suppressed in *TSC2*-Null NPCs, and their translation were reversed upon RMC-6272 or eFT-508 treatment. Our study here establishes the importance of mTORC1-eIF4F and MNK-eIF4E-mediated mRNA translation in TSC, ASD and other neurodevelopmental disorders and lay the groundwork for evaluating drugs in clinical development that target these pathways as a treatment strategy for TSC as well as ASD/NDD.

## INTRODUCTION

Tuberous sclerosis complex (TSC [MIM: 191100 and MIM: 613254]) is an autosomal dominant neurodevelopmental disorder showing clinical manifestations in multiple organ systems including the central nervous system (CNS). TSC is caused by mutations in the *TSC1*

55 [MIM: 605284] or *TSC2* [MIM: 191092] genes, encoding the tumor suppressor proteins
56 hamartin (TSC1) and tuberin (TSC2), respectively. In addition to slow growing hamartomas in
57 many organs, neurodevelopmental (ND) defects such as epilepsy, intellectual disability and
58 autism spectrum disorders (ASD) are commonly observed in these patients. [1-3]. TSC proteins
59 function as a complex relaying signal from diverse cellular pathways to control mechanistic
60 target of rapamycin (mTOR, [MIM: 601231]) complex 1 (mTORC1) signaling. Loss of
61 TSC1/TSC2 proteins results in aberrant activation of mTORC1, which has led to first-
62 generation mTORC1 inhibitors, rapamycin analogs ("rapalogs"), emerging as a lifelong
63 therapy for TSC hamartomas [4-7]. Moreover, recent clinical trials reveal that rapalogs reduce
64 epilepsy in 40% of TSC patients [8]. In contrast, rapalogs are ineffective in treating TSC-
65 associated neuropsychiatric disorders (TAND) and autism [9; 10].

66 Among its many activities, mTORC1 signaling plays an essential role in protein synthesis
67 by regulating the efficiency whereby mRNAs are translated into proteins. Aberrant activation
68 of mTORC1, as seen with TSC1/TSC2 loss, leads to hyperphosphorylation of key substrates
69 controlling translation including eukaryotic translation initiation factor (eIF) 4E-binding proteins
70 (4E-BPs [MIM: 602223 and MIM: 602224]) and ribosomal protein p70S6 kinase (S6K [MIM:
71 608938]). In the unphosphorylated state, i.e. when mTORC1 activity is low, 4E-BPs bind and
72 sequester eIF4E [MIM: 133440]. This leads to reduced formation of the heterotrimeric eIF4F-
73 complex, a key factor for initiation of translation, comprised of eIF4E, eIF4G [MIM: 600495]
74 and eIF4A [MIM: 602641]. Activation of mTORC1 leads to phosphorylation of 4E-BPs and
75 thereby release of eIF4E, which promotes eIF4F-complex formation and stimulates 5' cap-
76 dependent translation (Fig. 1A). Phosphorylation of S6K protein affects protein synthesis and
77 ribosomal biogenesis via multiple mechanisms, including release of sequestered eIF4A via
78 phosphorylation/inactivation of programmed cell death 4 (PDCD4 [MIM: 608610]) (Fig. 1A)
79 reviewed in [11; 12]. Importantly, mTORC1 modulates translation, and thereby molds the
80 proteome, in a transcript-selective fashion depending on features in the 5' untranslated regions
81 (UTRs) of target mRNAs. Three main classes of transcripts showing translation paralleling

82 mTORC1 activity have been described: mRNAs with very short 5'UTRs, highly structured
83 5'UTRs and those with the 5′ terminal oligopyrimidine (5′ TOP) motif (reviewed in [13]).
84 Moreover, activation of mTORC1 is associated with suppressed translation of a set of mRNAs
85 commonly harboring upstream open reading frames in their 5'UTRs [14]. In addition,
86 phosphorylation of eIF4E at a single conserved serine (S209) by mitogen-activated protein
87 kinase-interacting kinase MNK1/2 [MIM: 606724 and MIM: 605069] also modulates translation
88 in a transcript selective fashion (Fig. 1A) [15; 16].

89 Although commonly used rapalogs efficiently suppress phosphorylation of S6K1 they only
90 marginally affect 4E-BP1 phosphorylation in many cell types, which is consistent with rapalogs
91 only partially inhibiting mTORC1 activity [17-19]. This prompted development of bi-steric, third-
92 generation mTOR inhibitors that link the mTORC1 affinity of rapamycin with a potent second-
93 generation active-site mTOR kinase inhibitor, resulting in reduced phosphorylation of both
94 S6K1 and 4E-BP1 [20]. A more recent third-generation mTOR inhibitor, RMC-6272 (a tool
95 compound for its clinical counterpart RMC-5552), shows dramatically improved mTORC1
96 selectivity while still efficiently reducing phosphorylation of both S6K1 and 4E-BP1 (Fig. 1A)
97 {Burnett, 2023 #1356;Lee, 2021 #1418}. Moreover, we demonstrated that RMC-6272 is
98 superior to rapamycin in durable inhibition the mTORC1-4E-BP1 axis and suppression of
99 tumor growth in patient-derived *NF2*-deficient models [21]. Furthermore, RMC-6272 has shown
100 strong anti-tumor activity either alone or when combined with other treatments in several
101 preclinical cancer models {Burnett, 2023 #1356;Lee, 2021 #1418}, and clinical trials using
102 RMC-5552 have offered preliminary data of anti-tumor activity at tolerated doses
103 (NCT04774952 and NCT05557292; [22]. Similarly, recently developed eFT-508 is a highly
104 potent and selective MNK1/2 inhibitor that effectively inhibits phosphorylation of eIF4E (Fig.
105 1A) [23] and is in phase 2 clinical trials for several cancer types (NCT02937675, NCT02605083
106 and NCT03258398).

107 While numerous global studies of mRNA levels ("transcriptomes") have been carried out
108 in patient-derived neuronal models of ASD [MIM 209850], TSC and other ND disorders,

109 studies of how mRNAs are translation is largely lacking. Furthermore, the effects on mRNA
110 translation from highly specific mTORC1 and MNK inhibitors such as RMC-6272 and eFT-508
111 in ND disorders have never been explored. Our recent studies employing polysome-profiling
112 to examine mRNA translation at a transcriptome-wide level in TSC1 patient-derived neural
113 progenitor cells (NPCs) uncovered *TSC1*-associated transcript-selective alterations in
114 translation. Importantly, translation of a subset of mRNAs encoding proteins related to synaptic
115 regulation or ASD were rapamycin-insensitive but showed RMC-6272-sensitive translation.
116 Interestingly, unlike rapamycin, RMC-6272 also reversed some of the early ND phenotypic
117 defects in *TSC1*-Null NPCs [24]. These findings are consistent with a key role of the mTORC1-
118 4E-BP1-eIF4E axis. Here, we determine the role of this axis in regulating mRNA translation
119 using CRISPR-modified, isogenic TSC2 patient-derived NPCs. Our results reveal a strong
120 overlap in dysregulated translation observed in *TSC1*-Null and *TSC2*-Null NPCs. Surprisingly,
121 genes previously associated with ASD and NDD were translationally suppressed in *TSC2*-Null
122 NPCs, and their translation was reversed upon RMC-6272 or eFT-508 treatment. These
123 results establish the importance of mTORC1-eIF4F and MNK-eIF4E-mediated mRNA
124 translation in TSC, ASD and ND disorders and lay the groundwork for evaluating drugs in
125 clinical development that target these pathways as a treatment strategy for TAND as well as
126 ASD/NDD.
127

128 **MATERIAL AND METHODS**

129 ***Human induced pluripotent stem cell derivation***

130 We previously reported collection of post-mortem subungal fibroma (SUF) tissue from a
131 female sporadic TSC2 patient, which was obtained through the pathology department and
132 approved by the Institutional Review Board at Massachusetts General Hospital. Detailed
133 genetic analysis of the patient SUF tissue, including exon-by-exon scanning of the entire
134 coding sequence of *TSC2* isoform 1 (NCBI accession NM_000548), identified a single
135 heterozygous (*TSC2*-Het) truncating nonsense mutation in *TSC2* exon 34 (originally reported

136 as coding exon 33; 4207delG, D1400fs>1410X). Further analysis of the SUF tissue for tumor
137 clonality and loss-of-heterozygosity (LOH) at multiple polymorphic chromosome 16 or *TSC2*
138 intragenic markers revealed a clonal tumor with no second-hit mutations or LOH [25]. For
139 culturing of primary *TSC2*-Het fibroblasts, SUF tissue was rinsed twice in Hank's Balanced
140 Salt Solution (Sigma) followed by mincing in high glucose DMEM (Gibco) containing 15% fetal
141 bovine serum (FBS; Sigma), 0.5 µg/ml fungizone (Life Technologies), 50 g/ml gentamicin (Life
142 Technologies), and 1x penicillin-streptomycin/L-glutamine (Cellgro). The tissue was then
143 digested in the same medium as above (without gentamycin) containing ~5 units collagenase
144 III (Fisher Scientific), for 30 min at $37^0$C. Digested tissue was then pelleted by centrifugation,
145 resuspended in high glucose DMEM (containing 15%FBS, 1x penicillin-streptomycin/L-
146 glutamine) and expanded for subsequent experiments. *TSC2*-Het cells were reprogrammed
147 using synthetic modified mRNA-based methods to obtain induced pluripotent stem cells
148 (iPSCs) as described [26; 27]. Briefly, cells were transfected by nucleofection (Amaxa
149 Nucleofector I) with *in vitro* transcribed mRNAs encoding *Oct4, Sox2, Klf4, c-Myc* and *Lin28*
150 (Stemgent). After single clone picking, iPSC colonies were cultured in feeder-free conditions
151 in Essential 8 medium (ThermoFisher) on plates coated with Geltrex (Gibco) using the "thin
152 gel method" according to the manufacturer's instructions. Colonies were passaged every 4-6
153 days with daily medium change.
154
155 ***CRISPR/Cas9-mediated generation of isogenic iPSC lines***
156 To generate both the corrected-wildtype (WT) and Null isogenic iPSC lines, CRISPR/Cas9
157 genome editing was performed employing *TSC2*-Het patient-derived iPSCs. To achieve gene
158 knock-in to correct the germline *TSC2* mutation, we followed the same cloning and transfection
159 strategy as we previously reported for *TSC1* corrected-WT iPSCs [28]. Briefly, using web-based
160 CRISPR-related tools developed by GenScript (https://www.genscript.com), we designed a
161 single guide RNA (sgRNA): 5'-GGACATCCTCGGGGACCCTG-3' targeting *TSC2* exon 34
162 (coding exon 33) along with an asymmetric donor sequence: 5'-

163 CCGAGGCCGACCAGGCAGCACTTTCCCCGTCCAGGGTCCCTGACTGTGACCGGGCCT
164 TAACCTCAGGGCTCAGCCGGCCCACGTCGGCCTTGTCCCCAGGGTCCCCGAGGATGT
165 CCTGCAGAGTCTGCAG-3' for homology-directed repair. Colonies were manually isolated,
166 and genomic DNA was extracted from a portion of each colony followed by PCR amplification
167 using primers TSC2-ex33F: 5'-CTGACAGGGGTTCTCTTTGG-3' and TSC2-ex33R: 5'-
168 TCCAGGGTCCCTGACTGTGA-3', and Sanger sequencing was performed using a nested
169 primer TSC2-ex33-seqF: 5'-TCGTCCTCAGTCTCCAGCC-3'. Screening by Sanger
170 sequencing identified one clone with successful correction back to WT. For generating the
171 *TSC2*-Null iPSC lines, we used a service provided by an independent company (Alstem Cell
172 Advancements). Briefly, *TSC2*-Het iPSCs were co-transfected using the Amaxa nucleo-
173 electroporation system with a pair of sgRNAs targeting *TSC2* exon 2 (coding exon 1) including
174 sgRNA-1: 5'-TGTTGGGACTGGGAACACCG-3' and sgRNA-2: 5'-
175 ACTCACTCTCAGTATTTCCG-3'. A total of 50 single clones were screened by PCR
176 amplification and Sanger sequencing using primers TSC2-F2: 5'-
177 CCATGGCCAAACCAACAAG-3' and TSC2-R2: 5'-ACCTGGTGCAAGACCAAA-3', with 3
178 homozygous *TSC2*-Null cell lines identified, all of which harbored the same 59 bp deletion in
179 *TSC2* exon 2 resulting in a frameshift/premature truncating mutation.
180
181 ***Differentiation of iPSCs into NPCs***
182 To generate neural progenitor cells (NPCs), *TSC2*-iPSCs, including the parental *TSC2*-
183 Het line, the single *TSC2*-WT clone and two of the three *TSC2*-Null clones (clones 5 and 39)
184 were differentiated using the directed monolayer differentiation protocol as we previously
185 reported for TSC1-NPCs [28; 29]. Briefly, iPSCs expressing the pluripotency marker TRA-1-60
186 were sorted and enriched using the MACS MicroBead cell sorting technology (Miltenyi Biotec).
187 Cells were cultured in neural induction medium (neurobasal medium supplemented with 1x
188 neural induction supplement (ThermoFisher)) for 7-9 days, followed by a second sorting for
189 cells expressing polysialylated-neural cell adhesion molecule (PSA-NCAM). The PSC-NCAM-

190 positive (+) cells then underwent a double-sorting to enrich for NPCs representing CD271(-)
191 /CD133(+) cells. NPCs were then cultured in neural expansion medium (1:1 neurobasal
192 medium:advanced DMEM/F12, 1x penicillin/streptomycin and 1x neural induction
193 supplements (ThermoFisher)). MAC sorting was performed using microbead kits for TRA-1-
194 60, PSA-NCAM, CD271 and CD133 (Miltenyi Biotec).
195
196 ***Immunocytochemistry***
197 To confirm successful derivation of iPSCs and NPCs, immunofluorescent staining was
198 carried out using antibodies for iPSC markers Oct4 (Santa Cruz Biotechnologies) and Nanog
199 (Abcam), or NPC markers Nestin (EMD Millipore) and Sox2 (R&D Systems) as previously
200 described [28; 29]. Briefly, cells were fixed with 4% PFA and then permeabilized and blocked in
201 a single step using PBS containing 4% normal goat serum (NGS)/0.1% Triton-X-100. Primary
202 antibodies were diluted into PBS containing 2% NGS/0.1% Triton-X-100. DAPI was used to
203 stain nuclei (Invitrogen) at 5 μg/ml. Coverslips were mounted in ProLong Gold antifade
204 Mountant (Invitrogen) and images were captured using a Nikon Eclipse TE2000-U microscope
205 and the NIS-Element BR 3.2 imaging software.
206
207 ***Immunoblot analysis***
208 Cells were lysed in RIPA lysis buffer (50 mM Tris (pH7.5) and 150 mM NaCl, 0.1% SDS,
209 0.5% sodium deoxycholate, 1% NP-40, 1x HALT phosphatase inhibitor cocktail (Pierce) and
210 1x protease inhibitor cocktail (Sigma)) as previously described [30; 31]. Protein lysates were
211 resolved on 4-12% or 10-20% Novex WedgeWell Tris-glycine gels (Invitrogen), transferred to
212 0.45 μm pore nitrocellulose (BioRad) and then incubated with primary antibodies to detect
213 TSC2, pS6K T389, S6K, pS6 S240/244, S6, p4E-BP1 S65, 4E-BP1, peIF4E S209, and eIF4E
214 (Cell Signaling Technologies), β-actin (Santa Cruz Biotechnology) or GAPDH (EMD Millipore).
215 All immunoblotting data shown are representative of at least 3 biological replicates.
216

217 ***Cell Size and proliferation***

218 Cell size and proliferation rate were determined for *TSC2*-WT, Het and Null NPCs treated
219 for 72 h with 50 nM rapamycin, 10 nM RMC-6272 or DMSO as vehicle control. For both cell
220 size and proliferation, NPCs were analyzed by trypan blue exclusion using the Countess II
221 automated cell counter (ThermoFisher) as previously described [24; 28]. Briefly, cells were
222 detached using Accutase enzyme detachment medium (ThermoFisher), and for each sample,
223 10 µl of suspended cells were combined with 10 µl of trypan blue, and 10 µl of the resulting
224 mixture was assessed using the Countess II automated cell counter (ThermoFisher),
225 according to the manufacturer's instructions. Quantification of viable and dead cells was
226 performed along with size of viable cells. For proliferation, counting of viable cells collected at
227 days (D) 1, 2, 3 and 4 after seeding was performed for cells treated with 50 nM rapamycin, 10
228 nM RMC-6272 or DMSO on D1. All data collected using the Countess II cell counter were
229 analyzed from 3 independent experiments (3 technical replicates each). Proliferation was
230 further assessed using flow cytometry employing the proliferation marker Ki-67 as previously
231 described [24]. Briefly, *TSC2*-WT, Het and Null NPCs were seeded onto Geltrex-coated plates
232 followed by treatment with 50 nM rapamycin, 10 nM RMC-6272, 50 nM eFT-508 or DMSO as
233 vehicle control for 72 h (two biological replicates). To assess the Ki-67 proliferation status,
234 NPCs were fixed with 4% PFA, permeabilized with ice cold 100% methanol to a final
235 concentration of 90% with gentle vortexing and stained using AlexaFluor488-conjugated Ki-
236 67 monoclonal antibody or AlexFluor488-conjugated IgG as an isotype control (Cell Signaling
237 Technologies). Data were acquired from ~$1x10^4$ cells using a BD LSR II Flow Cytometer (BD
238 Biosciences), and analysis was carried out using FlowJo 10.8.1 (FlowJo LLC). Percentages
239 of Ki-67 positive cells (acquired through FITC channel) were determined by gating with respect
240 to Alexa488-IgG control.

241

242 ***Neurite outgrowth assay***

243 NPCs were assessed for neurite outgrowth as previously described [28]. Briefly, NPCs were
244 seeded on coverslips coated with poly-D-lysine (0.1 mg/ml, Sigma) and fibronectin (5 μg/ml,
245 Corning) in growth factor-depleted neural expansion medium containing 1:1 neurobasal
246 medium:advanced DMEM/F12 (ThermoFisher), 1x penicillin/streptomycin and 0.3x neural
247 induction supplements (ThermoFisher). Cells were treated with 50 nM rapamycin, 10 nM of
248 RMC-6272 or DMSO vehicle control for 48 h followed by fixation with 4% PFA prior to
249 immunostaining. Three independent experiments were performed where images were
250 acquired from 8 non-overlapping fields and analyzed using HCA-Vision software V.2.2.0
251 (CSIRO, Canberra, Australia) to determine (i) number of cells; (ii) average neurite
252 outgrowth/cell (total length), (iii) average number of neurites/cell and (iv) average number of
253 extremities/cell (number of termination points) [32]. Images were acquired using a Nikon Eclipse
254 TE2000-U microscope and the NIS-Element BR 3.2 imaging software.
255
256 ***Polysome fractionation and RNA sequencing***
257 Lysate were prepared for polysome profiling from three biological replicates as previously
258 described with minor modifications [33]. Briefly, TSC2-NPC lines were seeded at ~50,000
259 cells/cm$^2$, with a total of ~2.4x10$^7$ cells seeded per replicate for three drug treatment
260 conditions, including 10 nM RMC-6272, 50 nM EFT-508 or DMSO control. The day after
261 seeding, cells were treated for 2 h, rinsed with 1x PBS containing 100 µg/ml cycloheximide
262 (CHX) (Sigma), harvested by scraping on ice in PBS/CHX and pelleted by centrifugation at
263 300g for 10 min at + 4C. Cell pellets were first resuspended in hypotonic lysis buffer containing
264 5 mM Tris-HCl (pH 7.5), 2.5 mM $MgCl_2$ and 1.5 mM KCl, followed by addition of DTT (2 mM
265 final), CHX (100µg/ml final), sodium deoxycholate (0.5% final) and Triton X-100 (0.5% final).
266 Lysates were then vortexed for 4 sec, cleared by spinning for 2 min at 13,000 rpm and quickly
267 frozen on dry ice. When ready for processing, lysates were quickly thawed at 37C and loaded
268 onto a 10–50% sucrose gradient, followed by centrifugation for 2 h and 15 min at 35,000 rpm
269 in a SW41 rotor using a Sorvall Discovery 90SE centrifuge. The gradients were fractionated

270 on a Teledyne ISCO Foxy R1 apparatus while monitoring the OD254nm. Fractions
271 corresponding to mRNA associated with more than two ribosomes were pooled and the RNA
272 extracted using TRIzol (ThermoFisher) according to the manufacturer's protocol. 10% of the
273 lysate was removed from the extract prior to loading on the sucrose gradient, extracted using
274 TRIzol, and denoted as total RNA. RNA sequencing libraries were prepared from the resulting
275 samples (both polysome-associated and total RNA) using Illumina v2.5 Kits and sequenced
276 on an Illumina NextSeq 500 at the Canada's Michael Smith Genome Sciences Centre (BC
277 Cancer Research Institute, Vancouver, Canada).
278
279 ***RNA-seq data preprocessing and quality control***
280 Adapters were removed from RNA sequencing reads using bbduk.sh from the BBTools
281 software suite [https://www.osti.gov/servlets/purl/1241166] (v. 36.59 with settings: k = 13, ktrim
282 = n, useshortkmers = t, mink = 5, qtrim = t, trimq = 10, minlength = 20). Paired-end reads were
283 aligned to hg38 using HISAT2 [34] (ver 2.1.0 with settings: --no-mixed, --no-discordant), and
284 uniquely mapped reads were quantified using the featureCounts function from the RSubreads
285 package (v.2.6.4) [35] with RefSeq gene definitions and default settings. Polysome-profiling data
286 from our previous study of TSC1-dependent translation[24] was quantified using the same gene
287 definitions to allow a direct comparison to the herein generated dataset. Dataset reproducibility
288 was assessed using Principal Component Analysis using genes within highest quartile of
289 standard deviations quantified across all samples as input.
290
291 ***Analysis of gene expression alterations using anota2seq***
292 Gene expression quantified from polysome-associated and total mRNA were analyzed using
293 the anota2seq algorithm (v. 1.20.0) [36]. Batch effects were accounted for in the models by
294 including sample replicates using the "batchVec" argument in anota2seq. Default threshold
295 settings were used [settings minSlopeTranslation = - 1, maxSlopeTranslation = 2,
296 minSlopeBuffering = -2, maxSlopeBuffering = 1, deltaPT = deltaP = deltaTP = deltaT =

297 log2(1.2), minEff=log2(1.5)] with a significance threshold maxRvmPAdj = 0.15 (corresponding
298 to an FDR < 0.15). Transcripts were classified into three modes of regulation assessed by
299 anota2seq (changes in mRNA abundance, changes in translation, and translational offsetting)
300 using the "anota2seqRegModes' function.
301
302 ***Analysis of gene signatures using empirical cumulative distribution functions***
303 Empirical cumulative distribution functions (ECDFs) of log2 fold changes for polysome-
304 associated and total mRNA were plotted for gene signatures (ASD and NDD genes [37], eIF4E
305 overexpression [38], mTOR sensitive genes [39] obtained from previous publications or to cross-
306 compare datasets that were found to be translationally regulated in either dataset. The
307 Wilcoxon rank-sum test was used to determine whether there was a significant shift between
308 each signature and the background (i.e. genes not within the signature).
309
310 ***Analysis of enrichment of gene sets***
311 Gene Ontology (GO) enrichment analysis was performed using genes classified as
312 regulated via translation by anota2seq (differentially translated genes "DTGs") and annotation
313 from GO biological process (GO:BP) terms retrieved from MSigDB database (v. 2023.2.Hs) [40]
314 using one-tailed Fisher's exact test. In this analysis, only GO:BP terms with at least 10 genes
315 within in the background set (all detected genes analyzed by anoat2seq) of a particular
316 comparison were considered. DTG datasets for GO analysis included *TSC2*-Null vs WT
317 NPCs, *TSC2*-Null NPCs treated with RMC-6272 vs DMSO control, *TSC2*-Null NPCs treated
318 with eFT508 vs DMSO control, pairwise comparison between *TSC2*-Null NPCs treated with
319 RMC-6272 or eFT508 as well as pairwise comparison between *TSC2*-Null vs WT NPCs and
320 our previously published dataset for *TSC1*-Null vs WT NPCs [24].
321 Enrichment analysis for selected DTGs identified by anota2seq and target gene sets,
322 including ASD-, NDD-, EPI-associated genes [37; 40; 41] and eIF4E-sensitive genes [38], was
323 performed using one-tailed Fisher's exact test. Statistical significance of overlaps between the

324 two DTG datasets was also assessed using one-tailed Fisher's exact test. Here, all anota2seq
325 analyzed genes in a single comparison, or intersection of anoat2seq analyzed genes in paired
326 comparisons, constituted the background sets. These enrichment analyses were performed
327 in the R statistical software environment (version 3.4.3) (https://www.R-project.org/) using
328 custom scripts.
329
330 ***Validation of differential translation using RT-qPCR***
331 For validation, polysome fractionations were collected from *TSC2*-Null or *TSC2*-WT NPCs
332 (three biological replicates), and RNA was isolated as described for NPCs above. cDNA was
333 prepared using M-MuLV Reverse Transcriptase (New England Biolabs, Ipswich, MA) and
334 oligo(dT)20 primers using the manufacturer's recommendations. RT-qPCRs were performed
335 with SsoFast EvaGreen Supermix (Bio-Rad, Hercules, CA) using the CFX96 PCR system (Bio-
336 Rad Hercules, CA). Primers for RT-qPCR are detailed in Supplemental Table S1. The level of
337 each mRNA was normalized to β-actin (*ACTB*) and Phosphoglycerate Kinase 1 (*PGK1*) using
338 the comparative CT method and compared across conditions as indicated in the figure legend.
339
340 ***Statistical analyses***
341 Methods for statistics are described above, or in corresponding figure legends.
342
343 **RESULTS**
344 ***Generation and characterization of an isogenic set of TSC2 patient-derived neural***
345 ***progenitor* cells**
346 We generated an isogenic set of TSC2 patient-derived NPCs using a similar approach as
347 we described previously for TSC1 patient-derived NPCs [24; 28]. Primary fibroblasts cultured from
348 post-mortem SUF tissue were found to harbor a germline heterozygous 1 bp deletion in *TSC2*
349 exon 34 (originally reported as coding exon 33) with no loss of heterozygosity [25]. Induced
350 pluripotent stem cells (iPSCs) were generated from the fibroblasts, followed by CRISPR-

351 based genome editing to (i) correct the heterozygous mutation back to wildtype, or (ii) knock
352 out the second allele by introducing a 59 bp deletion in *TSC2* exon 2 (coding exon 1), both of
353 which were confirmed by Sanger sequencing (data not shown). This resulted in an isogenic
354 set of iPSCs representing the parental *TSC2*-Het line, a single clone for *TSC2*-corrected
355 (*TSC2*-WT) and three clones for *TSC2*-Null iPSCs. We then selected *TSC2*-WT, Het and two
356 iPSC clones (clones 5 and 39) for microbead sorting of neural cell surface protein markers to
357 obtain NPCs as previously described [28]. Immunostaining for neural markers Nestin and Sox2
358 confirmed successful NPC derivation (Supplemental Fig. S1A). Loss of TSC2 protein
359 expression was confirmed in *TSC2*-Null clones when compared with the TSC2-WT. We
360 observed increased phosphorylation of mTORC1 targets p70S6K (pS6K T389), pS6 S240/244
361 and p4E-BP1 S65 in both *TSC2*-Null NPC clones compared with *TSC2*-WT NPCs, consistent
362 with activation of mTORC1 signaling. *TSC2*-Het NPCs revealed only minimal activation of
363 mTORC1, which is in agreement with many previous reports that employed human iPSC
364 models of TSC [42-45] (Supplemental Fig. S1B). *TSC2*-Null NPCs demonstrated an enlarged cell
365 phenotype compared with *TSC2*-WT cells (Fig. 1B, D), which is a hallmark of mTORC1
366 activation. *TSC2*-Het NPCS exhibited an intermediate cell size phenotype (Fig. 1B, D).
367 Treatment with rapamycin or RMC-6272 attenuated phosphorylation of S6K at T389, along
368 with its downstream substrate ribosomal protein S6 (pS6 S240/244) and rescued the enlarged
369 cell size (Fig. 1C-D). As expected, rapamycin showed only minimal effects on phosphorylation
370 of 4E-BP1 while RMC-6272 demonstrated complete inhibition (Fig. 1C). These results are
371 consistent with our observations in TSC1-NPCs [24] and with previous studies showing that the
372 mTORC1-S6K signaling axis controls cell size [46].
373
374 ***Rescue of early neurodevelopmental phenotypes by RMC-6272, but not rapamycin***
375 We previously demonstrated that defects in early ND phenotypes in *TSC1*-Null NPCs,
376 including increases in proliferation rate and neurite outgrowth, could be rescued by RMC-6272
377 treatment but not rapamycin. This suggests dependence, at least in part, on the mTORC1-4E-

378 BP1 signaling axis [24; 28]. Here, we assessed proliferation by viable cell count in TSC2-NPCs
379 over the course of four days (D1-4) after seeding, along with 72 h treatment with 50 nM
380 rapamycin, 10 nM RMC-6272 or DMSO control initiated at D1. We observed genotype-
381 dependent cell numbers whereby *TSC2*-Null NPCs showed increased proliferation relative to
382 *TSC2*-Het and *TSC2*-WT NPCs while *TSC2*-Het had augmented proliferation as compared to
383 *TSC2*-WT NPCs (Fig. 2A, left graph region). When compared with DMSO treatment,
384 rapamycin showed no significant effect in TSC2-NPCs (Fig. 2A, center); whereas RMC-6272
385 demonstrated significant reduction by D3 in all three NPC genotypes, with the maximal
386 decrease observed in *TSC2*-Null NPCs (Fig. 2A, compare left and right graph regions).
387 Consistently, flow cytometry-based analysis showed a reduction in the percentage of S-
388 positive cells in RMC-6272 vs DMSO treated *TSC2*-WT (50.9% vs 62.7%), *TSC2*-Het (56.2%
389 vs 64.9%) and *TSC2*-Null (53.7% vs 68.9%) NPCs. In contrast, similar percentages of Ki-67
390 positivity were found for rapamycin or DMSO treatment (Supplemental Fig. S2A). Moreover,
391 treatment with eFT508/tomivosertib, a MNK1/2 inhibitor, which attenuates phosphorylation of
392 eIF4E at S209 (peIF4E S209) but not 4E-BP1 (p4E-BP1 S65) did not alter Ki-67 positivity in
393 *TSC2*-Null NPCs (Supplemental Fig. S2A and B).
394 We next studied neurites in our isogenic set of TSC2-NPCs using MAP2 immunostaining
395 and HCA-Vision image analysis software to, per cell, quantitate three parameters: (i) length of
396 neurite outgrowth, (ii) number of neurite roots and (iii) number of extremities (terminal endpoint
397 of primary and branched outgrowths). In TSC2-NPCs treated for 48 h with DMSO, a significant
398 increase in neurite length of ~3.2-fold in *TSC2*-Null and an intermediate increase of ~1.4-fold
399 in *TSC2*-Het was observed relative to *TSC2*-WT NPCs (Fig. 2B-C). *TSC2*-Null NPCs also
400 revealed a significant increase in neurite number (~1.5-fold) and extremities (~1.7-fold)
401 relative to *TSC2*-WT NPCs (Fig. 2B and C). Upon RMC-6272 treatment, we observed
402 decreases in neurite length, number and extremities of 0.73, 0.90 and 0.83, respectively, for
403 *TSC2*-Het NPCs, and 0.46, 0.68 and 0.64, respectively, for *TSC2*-Null NPCs (Fig. 2D). Similar
404 to the proliferation assays, rapamycin failed to rescue neurite-related phenotypes, and in fact

405 showed an opposite trend in several parameters (Fig. 2D). Taken together, these data support
406 that the third-generation mTORC1 inhibitor RMC-6272 is superior to rapamycin in reversing
407 the early ND phenotypes proliferation and neurite phenotypes in NPCs and that this depends
408 on the more potent inhibition of mTORC1 downstream targets including 4E-BP1.
409
410 ***Abundant mRNA translation alteration in* TSC2*-Null NPCs largely overlap with those***
411 ***observed in* TSC1*-Null NPCs***
412 Our findings above demonstrate activation of mTORC1 signaling and increases in
413 proliferation and neurite outgrowth in *TSC2*-Null NPCs, compared with WT cells. As mRNA
414 translation is a major downstream target of mTORC1, it is necessary to study how both mRNA
415 levels and translation are affected by loss of *TSC2* to disentangle gene expression-dependent
416 effects on cellular phenotypes. We therefore applied polysome-profiling in *TSC2*-Null and
417 *TSC2*-WT NPCs. During polysome-profiling, cytoplasmic mRNA is fractionated based on
418 ribosome-association and the resulting polysome-associated (mRNA associated with >2
419 ribosomes) and total cytoplasmic mRNA pools are then quantified using RNA sequencing
420 followed by anota2seq analysis [36; 47]. This allows identification of *TSC2*-associated alterations
421 in (i) "translation", defined as polysome-associated mRNA alterations not paralleled by
422 corresponding changes in total mRNA levels; (ii) "abundance", representing congruent
423 modulation of total and polysome-associated mRNA; and (iii) "offsetting", defined as
424 alterations in total mRNA not paralleled by corresponding changes in polysome-associated
425 mRNA. This analysis revealed numerous *TSC2*-associated alterations in mRNA translation
426 visualized using a scatterplot comparing *TSC2*-dependent changes in polysome-associated
427 and total mRNA (Fig. 3A, Supplemental Table S4) and densities of p-values and FDRs
428 obtained from anota2seq analysis (Fig. 3B). These alterations in translation occurred
429 alongside less abundant changes in mRNA levels and essentially in absence of translational
430 offsetting (Fig. 3A). Although the analysis is expected to be hampered by the large number of
431 regulated genes, we used gene ontology analysis to identify cellular functions targeted by

432 these changes in translation. This revealed that translationally suppressed transcripts encode
433 proteins enriched for annotation to cellular functions including protein DNA complex
434 organization, chromatin remodeling, RNA metabolism, and cell cycle while those involved in
435 a variety of metabolic processed were translationally activated (Fig. 3C).

436 To assess how these *TSC2*-associated alterations in mRNA translation compares to our
437 previously described *TSC1*-associated changes, we looked for differences in the response to
438 loss of *TSC1* vs *TSC2* relative to their respective control conditions (i.e. the interaction effect)
439 using an anota2seq-like approaches we described previously [48]. Strikingly, only one gene
440 showed a statistically significant difference in translation response upon *TSC1* vs *TSC2* loss
441 (at FDR < 0.15), and this analysis therefore argues for largely overlapping effects on mRNA
442 translation. To further assess this, we generated gene signatures of transcripts that were
443 translationally up or downregulated in *TSC1*-Null or *TSC2*-Null NPCs relative to their controls
444 and visualized how these gene sets were regulated across the two models. This revealed that
445 transcripts whose translation was activated or suppressed in *TSC2*-Null NPCs showed similar
446 regulation in *TSC1*-Null NPCs and, vice versa, transcripts whose translation were activated or
447 suppressed in *TSC1*-Null NPCs showed similar regulation in *TSC2*-Null NPCs (Fig. 3D). Yet,
448 there were differences in mRNA level changes for these subsets (compare Fig. 3D left and
449 right plots) that, together with expected threshold-effects, resulted in a smaller set of 949
450 translationally suppressed and 189 translationally activated transcripts passed threshold
451 applied in anota2seq for both comparisons (Fig. 3E). As expected, these shared genes were
452 enriched in similar gene ontology categories as those identified upon *TSC2* loss (Fig. 3F). In
453 aggregate, these results indicated extensive remodeling of mRNA translation in *TSC2*-Null
454 NPCs largely recapitulating that observed in *TSC1*-Null NPCs.

455

456 ***Suppressed translation of mRNAs encoding proteins associated with ASD and NDD***
457 ***upon* TSC2 *loss***

458 To explore the relationship between altered gene expression associated with *TSC2* loss
459 and patient phenotypes we reasoned that *TSC2* loss may affect translation of mRNAs
460 encoding proteins implicated in non-syndromic autism spectrum disorder (ASD), general
461 neurodevelopmental disorders (NDD) and/or epilepsy. To assess this, we utilized data from
462 recent studies that identified high confidence *de novo* mutations in large cohorts of individuals
463 diagnosed with ASD, NDD as well as epilepsy. For ASD/NDD-related genes, we used datasets
464 reported by Fu and colleagues, including 72 genes associated with ASD (ASD72) and 373
465 genes associated with NDD (NDD373) identified at a stringent FDR $\leq$ 0.001 threshold, as well
466 as 185 ASD-associated genes (ASD185) and 664 NDD-associated genes (NDD664) identified
467 at reduced stringency (FDR $\leq$ 0.05) [37]. For epilepsy-related genes, we used genes identified
468 in the Epi25 Collaborative, [41] that consists of 83 genes identified at p $\leq$ 0.005 by whole-exome
469 sequencing (case-control study) in the full epilepsy cohort (EPI). We next assessed whether
470 expression of ASD-, NDD- and epilepsy-associated genes are regulated in *TSC2*-Null NPCs
471 as determined by anota2seq analysis (i.e. from Fig. 3A). This analysis revealed strong
472 enrichment of ASD72 (~43% of all ASD72 genes; p = $1.72 \times 10^{-7}$) and NDD373 (~37% of all
473 NDD273 genes; p = $2.59 \times 10^{-19}$) genes among translationally suppressed transcripts as
474 compared to background (Table 1). This finding was further substantiated by applying two
475 approaches that do not use thresholds to identify sets of differentially regulated genes: i) gene
476 set enrichment analysis (GSEA) [40] (Fig. 4A); and ii) the same method as applied for *TSC1* vs
477 *TSC2* (i.e. Fig. 3D) gene subset-comparisons (Fig. 4B, top). Both these approaches showed
478 strong enrichment of ASD72 and NDD373 genes among transcripts translationally suppressed
479 in *TSC2*-Null as compared to isogenic WT NPCs. Similarly, in *TSC2*-Null NPCs, strong
480 enrichments among translationally suppressed genes were observed for the larger ASD185
481 and NDD664 gene sets **(**Supplemental Table S2A, Supplemental Fig. S3A and B**)** as well as
482 genes translationally suppressed in both *TSC2*-Null and *TSC1*-Null NPCs relative to their
483 respective controls (i.e. genes from Fig. 3E; Supplemental Table S2B**)**. A similar analysis for
484 EPI-associated genes revealed a smaller enrichment (~27% of all EPI-associated genes; p =

485 $5.82x10^{-3}$) (Table 1, Supplemental Fig. S3C and D) that was not confirmed using methods that
486 do not use thresholds to identify regulated sets of genes.
487 To ensure that this unexpected translational suppression of ASD- and NDD-associated
488 genes in NPCs occurs in the presence of expected effects on mRNA translation from mTORC1
489 activation, we applied the same approaches described above to sets of transcripts whose
490 translation was altered following overexpression of eIF4E [38]. Consistent with activation of the
491 mTORC1-eIF4F translational axis in *TSC2*-Null NPCs, there was a strong overlap between
492 genes whose translation was activated upon eIF4E-overexpression and *TSC2* loss
493 (Supplemental Table S3). A similar result was obtained when only considering genes that
494 were identified as translationally regulated by anota2seq following both *TSC1* and *TSC2* loss
495 (i.e. from Fig. 3E) and when a method not relying on thresholds was used (Fig. 4B, middle) as
496 well as for an additional signature of mTORC1-sensitive translation reported previously [14](Fig.
497 4B, bottom). Therefore, surprisingly, genes associated with ASD and NDD are largely
498 translationally suppressed in NPCs following inactivation of *TSC2* and these changes in
499 translation occur in parallel with activation of mTORC1-sensitive translation.
500
501 ***5'UTRs of ASD and NDD genes resemble those of mRNAs whose translation is***
502 ***suppressed upon activation of mTORC1***
503 The above results unveiled that translation of mRNAs encoding proteins associated with
504 ASD and NDD are affected by the activity of mTORC1. As mTORC1-sensitive translation
505 largely relies on features in the 5' untranslated region (5'UTR), this suggests that the observed
506 suppressed translation of ASD- and NDD-associated genes may depend on their 5'UTRs. As
507 discussed above, mRNAs whose translation parallels activity of mTORC1 often have short
508 and/or highly structured 5'UTRs and lack upstream open reading frames (uORFs). Strikingly,
509 ASD- and NDD-associated genes showed an opposite profile for 5'UTR length, GC-content
510 (which associates with secondary structures of the 5'UTR) and uORFs that was similar to
511 mRNAs whose translation was suppressed upon *TSC2* loss (Fig. 4C-E). Therefore, ASD- and

512 NDD-associated genes largely show 5'UTRs that are consistent with translational suppression
513 following increased activation of mTORC1.
514
515 ***RMC-6272 and eFT-508 reverse translationally suppressed* TSC2*-dependent***
516 ***transcripts and ASD and NDD genes***
517 The findings above suggest that suppressed translation of ASD- and NDD-associated
518 genes following loss of *TSC2* may be important for ND manifestation. Furthermore, this raises
519 the possibility that inhibition of mTORC1 signaling, or potentially other key pathways
520 modulating translation, may reverse *TSC2*-dependent translation of ASD- and NDD-
521 associated genes. To assess this, we performed polysome-profiling in *TSC2*-Null NPCs
522 treated with the bi-valent mTORC1 inhibitor RMC-6272, or the MNK1/2 inhibitor eFT-508. The
523 resulting dataset was analyzed as described above using anota2seq to determine how these
524 agents modulate gene expression. Both treatments resulted in dramatic mRNA translation
525 changes as visualized in scatterplots comparing effects in polysome-associated and total
526 mRNA levels as well as p-value and FDR densities (Supplemental Fig. S4A-D). Next, we
527 generated gene signatures of transcripts that were translationally increased or decreased in
528 *TSC2*-Null NPCs treated with RMC-6272 relative to DMSO control and compared how these
529 gene sets were regulated in *TSC2*-Null NPCs treated with eFT-508 vs DMSO control. This
530 revealed that transcripts whose translation was activated or suppressed by RMC-6272
531 showed similar regulation upon eFT-508 treatment and, vice versa, transcripts whose
532 translation was activated or suppressed by eFT-508 showed similar regulation upon RMC-
533 6272 treatment (Fig. 5A and B). To determine whether the agents reversed *TSC2*-sensitive
534 translation, we used the same strategy as above when comparing *TSC1*- vs *TSC2*-sensitive
535 translation (i.e. Fig. 3D). This revealed that both RMC-6272 as well as eFT-508 partially
536 reversed *TSC2*-sensitive translation (Fig. 5C). Gene ontology analysis of genes overlapping
537 in *TSC2*-Null NPCs treated with RMC-6272 or eFT-508 revealed significant reversal of some
538 enriched annotations related to cellular functions that were identified as *TSC2*-dependent

539 (shown in Fig. 3C), including positive regulation of transcription by RNA polymerase II, positive
540 regulation of RNA metabolic process and protein DNA complex organization along with
541 transcripts involved in various metabolic processes (Fig. 5D).

542 By comparing anota2seq outputs for these analyses we observed that, among all
543 transcripts whose translation was increased in *TSC2*-Null cells (Fig. 3A), 614 or 936 were
544 suppressed upon RMC-6272 or eFT-508 treatment, respectively, with an overlap of 513
545 transcripts; and 1454 or 1177 transcripts that were translationally suppressed in *TSC2*-Null
546 NPCs were translationally activated upon RMC-6272 or eFT-508 treatment, respectively, with
547 an overlap of 874 transcripts (all overlaps were statistically significant; Supplemental Fig. S4E,
548 Supplemental Table S4)**.** Gene ontology analysis of *TSC2*-dependent differentially translated
549 genes (from Fig. 3A) revealed significant reversal of enriched annotations upon treatment with
550 RMC-6272 or eFT-508 as well as reversal of key cellular functions shown in Fig. 3C
551 (Supplemental Fig. S4F and G).

552 Although the inhibitors led to altered translation of similar numbers of transcripts in *TSC2*-
553 Null NPCs, anota2seq analysis contrasting the two treatments revealed substantial
554 differences in terms of affected mRNAs (Supplemental Fig. S5A and B). This was further
555 substantiated by gene ontology analysis, which revealed that while RMC-6272 e.g. more
556 efficiently suppressed translation of mRNAs encoding proteins involved in translation and
557 oxidative phosphorylation, mRNAs showing relatively more suppressed translation after
558 eFT508 treatment were e.g. annotated to neuronal development (Supplemental Fig. S5C).

559 Next, we assessed whether translation of mRNAs encoding ASD- and NDD-associated
560 genes were affected by mTORC1 or MNK1/2 activity. This revealed a striking reversal in
561 translation of both ASD and NDD genes in *TSC2*-Null NPCs treated with RMC-6272 or eFT-
562 508 (Fig. 6A). To identify affected genes, we compared outputs from the corresponding
563 anota2seq analyses. Among the 31 ASD72 genes translationally suppressed in *TSC2*-Null
564 NPCs, 28 (~90%) and 18 (~58%) were translationally activated upon RMC-6272 (RMC-
565 responsive) and eFT508 treatment (eFT-responsive), respectively (while all eFT-responsive

566 genes were identified as RMC-responsive, 10 genes were only responsive to RMC-6272;
567 Table 1, Fig. 6B). Moreover, for translationally suppressed NDD373 genes, 96 (~70%) and 69
568 (50%) were RMC- and eFT-responsive (Table 1), respectively (60 were both RMC- and eFT-
569 responsive; similar results were obtained for ASD185 and NDD664 genes; Supplemental
570 Table S2A). To validate alterations in translation upon *TSC2* loss as well as reversal by the
571 inhibitors, we selected five ASD/NDD-associated genes that were translationally suppressed
572 in *TSC2*-Null NPCs: *SETD1B* [MIM: 611055], *DYRK1A* [MIM: 600855], *CHD8* [MIM: 610528],
573 *NRXN1* [MIM: 600565], and *TCF7L2* [MIM: 62228], and also five eIF4E-sensitive genes that
574 were translationally activated in *TSC2*-Null NPCs: *AP2S1* [MIM: 602242], *LZTR1* [MIM:
575 600574], *WDR54*, *ALDOC* [MIM: 103870], and *EIF2B2* [MIM: 606454]. Quantitative RT-PCR
576 (RT-qPCR) analysis from polysome-associated mRNA fractions (>2 ribosomes) adjusted for
577 alterations in total mRNA showed a reduction for all five ASD/NDD-related genes and
578 increases in all five eIF4E-sensitive genes in *TSC2*-Null vs WT NPCs, confirming the above
579 polysome-profiling results. Moreover, RMC-6272 or eFT508 reversed *TSC2*-dependent
580 translationally suppressed ASD/NDD and translationally activated eIF4E-sensitive genes (Fig.
581 6C).

582 Taken together, *TSC2*-dependent decreased translation of mRNAs associated with ASD
583 and NDD can be reversed upon RMC-6272 or eFT508 treatment. These results are intriguing
584 and potentially imply paradoxically suppressed translation of a subset of
585 neurodevelopmentally important genes that nonetheless depend on mTORC1-eIF4F pathway
586 activation.

587

588 **DISCUSSION**

589 The central role of mTORC1 signaling in translation initiation and protein synthesis in
590 a variety of cell types, including stem cells, as well as in human disease is well established [11;
591 49; 50]. While many transcriptome studies have been reported in *TSC1/2*-deficient neuronal cells,
592 how *TSC2* loss affects mRNA translation, particularly in patient-derived cells, is unknown. We

593 recently reported *TSC1*-dependent alterations in mRNA translation employing an isogenic set
594 of CRISPR-modified, TSC1 patient-derived NPCs. Although polysome-profiling revealed a
595 partial reversal of *TSC1*-associated gene expression changes following rapamycin treatment,
596 most genes related to neural activity/synaptic regulation or ASD remained rapamycin-
597 insensitive [24]. Here, we describe generation and characterization of an independent isogenic
598 set of CRISPR-modified NPCs from a TSC patient with a loss-of-function germline mutation
599 in *TSC2*. We find that *TSC2*-Null NPCs mimic *TSC1* loss in activation of mTORC1 signaling
600 and early ND phenotypic changes [24]. Rapamycin treatment of *TSC2*-Null NPCs fully inhibited
601 phosphorylation of S6K and reduced enlarged cell size but had minimal effects on 4E-BP1
602 phosphorylation and early ND phenotypes. In contrast, the third-generation mTORC1 inhibitor
603 RMC-6272 revealed efficient inhibition of both S6K and 4E-BP1 phosphorylation and rescued
604 the ND phenotypes as well as cell size. These data suggest that while enlarged cell size
605 observed upon *TSC2* loss depends on the mTORC1-S6K axis of the pathway, which is
606 consistent with previous reports [46], the altered ND phenotypes depend on the mTORC1-4E-
607 BP1 signaling axis.

608 We observed dramatic changes in mRNA translation associated with *TSC2* loss in NPCs
609 that largely overlapped with those observed upon *TSC1* loss. Provided that *TSC1* and *TSC2*
610 loss-assert similar effects on mTORC1 signaling, a substantial overlap is expected. Importantly
611 as the cells were derived from independent patients, our results support a robust effect on
612 mRNA translation across patients with hyperactive mTORC1 activity. In this study, in addition
613 to RMC-6272 that inhibits mTORC1 activity, we also considered alternative approaches to
614 modulate activity of the eIF4F complex and therefore included the MNK1/2 inhibitor
615 eFT508/tomivosertib to understand the convergence of mTORC1-4E-BP1 and MNK-eIF4E
616 signaling pathways on *TSC2*-dependent protein synthesis (see Fig.1A). While mTORC1-
617 sensitive translation has been studied extensively at the transcriptome-wide level [39; 51-53], the
618 understanding of how the MNK-eIF4E axis modulates mRNA translation at a global scale is
619 more limited [16]. This study is the first that includes a direct comparison between these

620 pathways toward mRNA translation and reveals that a large proportion of translational
621 alterations observed in *TSC2*-Null NPCs can be reversed by RMC-6272 or eFT-508, strongly
622 suggesting that these changes are indeed mediated by mTORC1-4E-BP1 and MNK-eIF4E
623 signaling via active eIF4F complex-dependent protein translation. However, the drugs are not
624 equivalent since RMC-6272 would be expected to affect both 4E-BP1-dependent and
625 MNK1/2-dependent translation whereas eFT-508 would be restricted to MNK1/2-dependent
626 translation. We also observe ample differences between the two drugs with respect to
627 translation, which are in line with previous studies showing differences in affected phenotypes
628 as the mTORC1-4E-BP1 axis is a key regulator of e.g. cell cycle progression [19; 54] while
629 MNK1/2-eIF4E controls e.g. cancer-associated phenotypes including cell migration [55; 56].
630 As epilepsy and ASD are strongly associated with TSC, we compared transcripts that were
631 differentially translated in *TSC2*-Null vs WT NPCs to recent genetic datasets available from
632 large cohorts of individuals with ASD, NDD and epilepsy [37; 41]. Interestingly, numerous non-
633 monogenic ASD-, NDD- and epilepsy-associated genes identified in patients harboring
634 putative loss-of-function mutations, including protein truncating or damaging missense
635 variants, were translationally suppressed in *TSC2*-Null NPCs and overlapped with data from
636 our previously reported *TSC1*-model. Notably, the results for ASD- and NDD-associated
637 genes were confirmed using multiple methods, which suggests that for these subsets there is
638 a strong negative regulatory effect on mRNA translation impacting a large proportion of these
639 mRNAs. This was not the case for epilepsy-associated genes, in that a smaller fraction of
640 these genes was translationally suppressed upon *TSC2* loss. Importantly, these decreases in
641 translation were observed side-by-side with the expected increased translation of mRNAs that
642 were previously reported to be translationally activated upon mTORC1 pathway activation.
643 This suppressed translation was, for a majority of identified ASD/NDD genes, reversed by
644 inhibition of mTORC1 using RMC-6272 or MNK1/2 using eFT-508. A recent elegant large-
645 scale transcriptome study demonstrated that CRISPR perturbation of several ASD genes
646 results in differential expression of ASD/NDD-related genes that positively correlate with co-

647 expression of the perturbed gene, thereby establishing a high level of convergence across
648 ASD risk genes [57]. Our results here showing translational suppression of many ASD/NDD
649 genes upon loss of *TSC2* is consistent with the positive correlation and co-expression reported
650 by Liao and colleagues [57]. However, most notably, our results demonstrate that a majority of
651 translationally suppressed ASD/NDD/epilepsy genes can be reversed by RMC-6272 or eFT-
652 508, thereby establishing the roles of mTORC1-4E-BP1 and MNK-eIF4E in regulating
653 translation of these genes.

654 Many of the translationally suppressed ASD genes are FMRP targets. FMRP was
655 originally considered to function as a translational repressor that can bind to numerous mRNAs
656 that are generally larger than average and enriched for genes associated with ID and ASD [58;
657 59]. However, recent studies of FMRP-deficiency document a decrease in translation initiation
658 rates of many FMRP targets including ASD-related genes, which contrasts the notion that
659 FMRP is solely a translational repressor and supports a model where FMRP can also function
660 to increase the translation initiation of many targets [60-63]. Furthermore, in *TSC2*-Null NPCs we
661 also observe that 32 translationally suppressed ASD/NDD-related genes are associated with
662 chromatin-remodeling [64; 65]. Additional studies are therefore necessary to fully comprehend
663 how the ASD- and NDD-associated genes are translationally suppressed upon loss of *TSC2*.

664 In the literature, a main focus has been towards understanding mechanisms underlying
665 transcript-selective translation paralleling mTORC1 activity [13] while less attention has been
666 given to transcript that show decreased translation upon mTORC1 activation. Translation of
667 mRNAs enriched for 5'UTRs containing uORFs are translationally suppressed upon mTORC1
668 activation [39]. Consistently, we observed an increased frequency of uORFs in both ASD- and
669 NDD-associated genes; however, it should be noted that uORFs are also common among
670 background transcripts, and a relatively large proportion of ASD- and NDD-associated genes
671 do not have uORFs in their 5'UTRs.

672 Our results raise the critical question as to how ASD/NDD-related genes are translationally
673 suppressed upon mTORC1 activation in *TSC2*-Null NPCs. In addition to mTORC1, the

674 integrated stress response (ISR), which selectively modulates translation of transcripts with
675 5'UTRs harboring uORFs [66], is a key regulator of mRNA translation. In response to cellular
676 stress, phosphorylation of eukaryotic translation initiation factor 2 alpha (eIF2$\alpha$) is increased
677 by stress sensing kinases, which leads to a decrease in global protein synthesis paralleled by
678 increased translation of mRNAs with 5'-uORFs including the transcription factor ATF4
679 (reviewed in [67]). A recent study that employed multiplexed enhanced protein dynamics mass
680 spectrometry has shown that activation of the ISR pathway by cellular stressors and inhibition
681 of mTORC1 by Torin1 share translatome changes with approximately 20% of the proteins
682 synthesized at reduced levels, demonstrating the convergence of the two pathways in
683 regulating translation of specific proteins [68]. In contrast, our results reveal that mTORC1
684 inhibition in fact reverses the translational downregulation of ASD/NDD genes upon mTORC1
685 activation in *TSC2*-deficient NPCs raising a question whether ISR signaling has any role in
686 TSC. The involvement of the ISR pathway in our TSC models clearly needs further
687 investigation.

688 Another potential mechanism of translational regulation is via microRNAs (miRNAs), which
689 are involved in ND disorders [69]. Among 31 translationally suppressed transcripts in *TSC2*-Null
690 NPCs that show strong association with ASD (ASD72, FDR<0.001), 28 are predicted to be
691 targeted by at least one miRNA, using the miTarBase 2017 library (data not shown).
692 Interestingly, of the individual miRNAs identified by miTarBase analysis, four (hsa-miR-27b-
693 3p, hsa-let-7g-3p, hsa-miR-29a-3p and hsa-miR-515-5p) were reported as increased upon
694 *TSC1*- or *TSC2*-shRNA suppression in human neural stem cells generated from skin
695 fibroblast-derived iPSCs ($p < 0.05$) [70]; and three (hsa-miR-21-5p, hsa-miR-19b-3p and hsa-
696 miR-144-3p) were shown to be overexpressed in human autism brain samples [71]. Based on
697 this, it is tempting to speculate that miRNAs may play a role in suppressing translation in
698 *TSC2*-Null NPCs, and future studies will address this mechanistic possibility.

699 In summary, we establish that loss of *TSC2* in patient-derived NPCs results in numerous
700 changes in mRNA translation, which significantly overlaps with loss of *TSC1*. Loss of *TSC2*

701 associates with suppressed translation of a large proportion of ASD- and NDD-related genes,
702 which is reversed by inhibition of mTORC1 or MNK1/2, demonstrating the importance of
703 eIF4F-dependent mRNA translation in ND disorders. Our work also supports the therapeutic
704 potential for RMC-5552 (the clinical counterpart of RMC-6272) and eFT508/tomivosertib that
705 are currently under clinical development for cancer, as a strategy for treatment of TAND as
706 well as ASD and other neurodevelopmental disorders.
707

708 **DECLARATION OF INTERESTS**

709 The authors declare no competing interests.
710

711 **ACKNOWLEDGEMENTS**

712 This paper is dedicated to the memory of the late Dr. Jerry Pelletier, a distinguished James
713 McGill Professor in the Department of Biochemistry and Oncology from the Goodman Cancer
714 Institute at McGill University, Montreal, Canada, who unfortunately passed away during the
715 completion of this study. This work was supported by NIH R01 NS109540 (V.R.), the Swedish
716 Brain foundation FO2022-0178 (O.L.); the Swedish research council 2020-01665 (O.L.); the
717 Wallenberg academy fellow program 2013.0181 (O.L.).
718

719 **AUTHOR CONTRIBUTIONS**

720 Conceptualization and study design: V.R. and O.L.; experimental methods and data
721 acquisition P.M., K.S., F.R., S.B., R.B., N.R., J.B., S.C. and I.N.; data analysis and
722 interpretation: P.M., K.S., F.R., S.B., R.B. S.C., I.N., S.H., S.E. and O.L.; manuscript
723 preparation and editing: P.M., K.S., F.R., S.B., R.B., I.N., S.H., S.E., O.L. and V.R.
724

725 **WEB RESOURCES**

726 OMIM, https://www.omim.org/
727 GenScript, https://www.genscript.com

728 BBTools software suite, https://www.osti.gov/servlets/purl/1241166

729 R statistical software environment, https://www.R-project.org/

730

731 **DATA AND CODE AVAILABILITY**

732 The polysome-profiling datasets supporting the conclusions of this article are included within
733 the article (and its additional file(s)), and the full datasets will be deposited into Gene
734 Expression Omnibus (GEO).

735

736 **REFERENCES**


737 1. de Vries, P.J., Heunis, T.M., Vanclooster, S., Chambers, N., Bissell, S., Byars, A.W., Flinn,
738 J., Gipson, T.T., van Eeghen, A.M., Waltereit, R., et al. (2023). International consensus
739 recommendations for the identification and treatment of tuberous sclerosis complex-
740 associated neuropsychiatric disorders (TAND). J Neurodev Disord 15, 32.

741 2. Henske, E.P., Jozwiak, S., Kingswood, J.C., Sampson, J.R., and Thiele, E.A. (2016).
742 Tuberous sclerosis complex. Nat Rev Dis Primers 2, 16035.

743 3. Sahin, M., Henske, E.P., Manning, B.D., Ess, K.C., Bissler, J.J., Klann, E., Kwiatkowski,
744 D.J., Roberds, S.L., Silva, A.J., Hillaire-Clarke, C.S., et al. (2016). Advances and
745 Future Directions for Tuberous Sclerosis Complex Research: Recommendations From
746 the 2015 Strategic Planning Conference. Pediatr Neurol 60, 1-12.

747 4. Bissler, J.J., McCormack, F.X., Young, L.R., Elwing, J.M., Chuck, G., Leonard, J.M.,
748 Schmithorst, V.J., Laor, T., Brody, A.S., Bean, J., et al. (2008). Sirolimus for
749 angiomyolipoma in tuberous sclerosis complex or lymphangioleiomyomatosis. N Engl
750 J Med 358, 140-151.

751 5. Davies, D.M., de Vries, P.J., Johnson, S.R., McCartney, D.L., Cox, J.A., Serra, A.L.,
752 Watson, P.C., Howe, C.J., Doyle, T., Pointon, K., et al. (2011). Sirolimus therapy for
753 angiomyolipoma in tuberous sclerosis and sporadic lymphangioleiomyomatosis: a

754 phase 2 trial. Clinical cancer research : an official journal of the American Association
755 for Cancer Research 17, 4071-4081.
756 6. Julich, K., and Sahin, M. (2014). Mechanism-based treatment in tuberous sclerosis
757 complex. Pediatric neurology 50, 290-296.
758 7. Krueger, D.A., Care, M.M., Holland, K., Agricola, K., Tudor, C., Mangeshkar, P., Wilson,
759 K.A., Byars, A., Sahmoud, T., and Franz, D.N. (2010). Everolimus for subependymal
760 giant-cell astrocytomas in tuberous sclerosis. The New England journal of medicine
761 363, 1801-1811.
762 8. Overwater, I.E., Rietman, A.B., van Eeghen, A.M., and de Wit, M.C.Y. (2019). Everolimus
763 for the treatment of refractory seizures associated with tuberous sclerosis complex
764 (TSC): current perspectives. Ther Clin Risk Manag 15, 951-955.
765 9. Krueger, D.A., Sadhwani, A., Byars, A.W., de Vries, P.J., Franz, D.N., Whittemore, V.H.,
766 Filip-Dhima, R., Murray, D., Kapur, K., and Sahin, M. (2017). Everolimus for treatment
767 of tuberous sclerosis complex-associated neuropsychiatric disorders. Ann Clin Transl
768 Neurol 4, 877-887.
769 10. Overwater, I.E., Rietman, A.B., Mous, S.E., Bindels-de Heus, K., Rizopoulos, D., Ten
770 Hoopen, L.W., van der Vaart, T., Jansen, F.E., Elgersma, Y., Moll, H.A., et al. (2019).
771 A randomized controlled trial with everolimus for IQ and autism in tuberous sclerosis
772 complex. Neurology 93, e200-e209.
773 11. Saba, J.A., Liakath-Ali, K., Green, R., and Watt, F.M. (2021). Translational control of stem
774 cell function. Nat Rev Mol Cell Biol 22, 671-690.
775 12. Thoreen, C.C. (2017). The molecular basis of mTORC1-regulated translation. Biochem
776 Soc Trans 45, 213-221.
777 13. Masvidal, L., Hulea, L., Furic, L., Topisirovic, I., and Larsson, O. (2017). mTOR-sensitive
778 translation: Cleared fog reveals more trees. RNA Biol 14, 1299-1305.

779 14. Gandin, V., Masvidal, L., Cargnello, M., Gyenis, L., McLaughlan, S., Cai, Y., Tenkerian,
780 C., Morita, M., Balanathan, P., Jean-Jean, O., et al. (2016). mTORC1 and CK2
781 coordinate ternary and eIF4F complex assembly. Nat Commun 7, 11127.
782 15. Bramham, C.R., Jensen, K.B., and Proud, C.G. (2016). Tuning Specific Translation in
783 Cancer Metastasis and Synaptic Memory: Control at the MNK-eIF4E Axis. Trends
784 Biochem Sci 41, 847-858.
785 16. Karampelias, C., Watt, K., Mattsson, C.L., Ruiz, A.F., Rezanejad, H., Mi, J., Liu, X., Chu,
786 L., Locasale, J.W., Korbutt, G.S., et al. (2022). MNK2 deficiency potentiates beta-cell
787 regeneration via translational regulation. Nat Chem Biol 18, 942-953.
788 17. Choo, A.Y., Yoon, S.O., Kim, S.G., Roux, P.P., and Blenis, J. (2008). Rapamycin
789 differentially inhibits S6Ks and 4E-BP1 to mediate cell-type-specific repression of
790 mRNA translation. Proceedings of the National Academy of Sciences of the United
791 States of America 105, 17414-17419.
792 18. Fan, Q.W., Nicolaides, T.P., and Weiss, W.A. (2018). Inhibiting 4EBP1 in Glioblastoma.
793 Clin Cancer Res 24, 14-21.
794 19. Larsson, O., Morita, M., Topisirovic, I., Alain, T., Blouin, M.J., Pollak, M., and Sonenberg,
795 N. (2012). Distinct perturbation of the translatome by the antidiabetic drug metformin.
796 Proc Natl Acad Sci U S A 109, 8977-8982.
797 20. Rodrik-Outmezguine, V.S., Okaniwa, M., Yao, Z., Novotny, C.J., McWhirter, C., Banaji, A.,
798 Won, H., Wong, W., Berger, M., de Stanchina, E., et al. (2016). Overcoming mTOR
799 resistance mutations with a new-generation mTOR inhibitor. Nature 534, 272-276.
800 21. Bhattacharyya, S., Oblinger, J.L., Beauchamp, R.L., Kosa, L., Robert, F., Plotkin, S.R.,
801 Chang, L.S., and Ramesh, V. (2024). Preclinical evaluation of the third-generation, bi-
802 steric mechanistic target of rapamycin complex 1-selective inhibitor RMC-6272 in NF2-
803 deficient models. Neurooncol Adv 6, vdae024.
804 22. Burnett, G.L., Yang, Y.C., Aggen, J.B., Pitzen, J., Gliedt, M.K., Semko, C.M., Marquez, A.,
805 Evans, J.W., Wang, G., Won, W.S., et al. (2023). Discovery of RMC-5552, a Selective

806 Bi-Steric Inhibitor of mTORC1, for the Treatment of mTORC1-Activated Tumors. J Med
807 Chem 66, 149-169.
808 23. Reich, S.H., Sprengeler, P.A., Chiang, G.G., Appleman, J.R., Chen, J., Clarine, J., Eam,
809 B., Ernst, J.T., Han, Q., Goel, V.K., et al. (2018). Structure-based Design of Pyridone-
810 Aminal eFT508 Targeting Dysregulated Translation by Selective Mitogen-activated
811 Protein Kinase Interacting Kinases 1 and 2 (MNK1/2) Inhibition. J Med Chem 61, 3516-
812 3540.
813 24. Aksoylu, I.S., Martin, P., Robert, F., Szkop, K.J., Redmond, N.E., Bhattacharyya, S.,
814 Wang, J., Chen, S., Beauchamp, R.L., Nobeli, I., et al. (2023). Translatome analysis
815 of tuberous sclerosis complex 1 patient-derived neural progenitor cells reveals
816 rapamycin-dependent and independent alterations. Mol Autism 14, 39.
817 25. Niida, Y., Stemmer-Rachamimov, A.O., Logrip, M., Tapon, D., Perez, R., Kwiatkowski,
818 D.J., Sims, K., MacCollin, M., Louis, D.N., and Ramesh, V. (2001). Survey of somatic
819 mutations in tuberous sclerosis complex (TSC) hamartomas suggests different genetic
820 mechanisms for pathogenesis of TSC lesions. Am J Hum Genet 69, 493-503.
821 26. Schlaeger, T.M., Daheron, L., Brickler, T.R., Entwisle, S., Chan, K., Cianci, A., DeVine, A.,
822 Ettenger, A., Fitzgerald, K., Godfrey, M., et al. (2015). A comparison of non-integrating
823 reprogramming methods. Nat Biotechnol 33, 58-63.
824 27. Warren, L., Manos, P.D., Ahfeldt, T., Loh, Y.H., Li, H., Lau, F., Ebina, W., Mandal, P.K.,
825 Smith, Z.D., Meissner, A., et al. (2010). Highly efficient reprogramming to pluripotency
826 and directed differentiation of human cells with synthetic modified mRNA. Cell Stem
827 Cell 7, 618-630.
828 28. Martin, P., Wagh, V., Reis, S.A., Erdin, S., Beauchamp, R.L., Shaikh, G., Talkowski, M.,
829 Thiele, E., Sheridan, S.D., Haggarty, S.J., et al. (2020). TSC patient-derived isogenic
830 neural progenitor cells reveal altered early neurodevelopmental phenotypes and
831 rapamycin-induced MNK-eIF4E signaling. Mol Autism 11, 2.

832 29. Sellgren, C.M., Gracias, J., Watmuff, B., Biag, J.D., Thanos, J.M., Whittredge, P.B., Fu,
833 T., Worringer, K., Brown, H.E., Wang, J., et al. (2019). Increased synapse elimination
834 by microglia in schizophrenia patient-derived models of synaptic pruning. Nat Neurosci
835 22, 374-385.
836 30. Han, S., Kim, S., Bahl, S., Li, L., Burande, C.F., Smith, N., James, M., Beauchamp, R.L.,
837 Bhide, P., Diantonio, A., et al. (2012). The E3 Ubiquitin Ligase Protein Associated with
838 Myc (Pam) Regulates Mammalian/Mechanistic Target of Rapamycin Complex 1
839 (mTORC1) Signaling in Vivo through N- and C-terminal Domains. The Journal of
840 biological chemistry 287, 30063-30072.
841 31. James, M.F., Han, S., Polizzano, C., Plotkin, S.R., Manning, B.D., Stemmer-Rachamimov,
842 A.O., Gusella, J.F., and Ramesh, V. (2009). NF2/merlin is a novel negative regulator
843 of mTOR complex 1, and activation of mTORC1 is associated with meningioma and
844 schwannoma growth. Molecular and cellular biology 29, 4250-4261.
845 32. Wang, D., Lagerstrom, R., Sun, C., Bishof, L., Valotton, P., and Gotte, M. (2010). HCA-
846 vision: Automated neurite outgrowth analysis. J Biomol Screen 15, 1165-1170.
847 33. Gandin, V., Sikstrom, K., Alain, T., Morita, M., McLaughlan, S., Larsson, O., and
848 Topisirovic, I. (2014). Polysome fractionation and analysis of mammalian translatomes
849 on a genome-wide scale. J Vis Exp.
850 34. Kim, D., Paggi, J.M., Park, C., Bennett, C., and Salzberg, S.L. (2019). Graph-based
851 genome alignment and genotyping with HISAT2 and HISAT-genotype. Nat Biotechnol
852 37, 907-915.
853 35. Liao, Y., Smyth, G.K., and Shi, W. (2019). The R package Rsubread is easier, faster,
854 cheaper and better for alignment and quantification of RNA sequencing reads. Nucleic
855 Acids Res 47, e47.
856 36. Oertlin, C., Lorent, J., Murie, C., Furic, L., Topisirovic, I., and Larsson, O. (2019). Generally
857 applicable transcriptome-wide analysis of translation using anota2seq. Nucleic Acids
858 Res 47, e70.

859 37. Fu, J.M., Satterstrom, F.K., Peng, M., Brand, H., Collins, R.L., Dong, S., Wamsley, B., Klei,
860 L., Wang, L., Hao, S.P., et al. (2022). Rare coding variation provides insight into the
861 genetic architecture and phenotypic context of autism. Nat Genet 54, 1320-1331.
862 38. Larsson, O., Li, S., Issaenko, O.A., Avdulov, S., Peterson, M., Smith, K., Bitterman, P.B.,
863 and Polunovsky, V.A. (2007). Eukaryotic translation initiation factor 4E induced
864 progression of primary human mammary epithelial cells along the cancer pathway is
865 associated with targeted translational deregulation of oncogenic drivers and inhibitors.
866 Cancer Res 67, 6814-6824.
867 39. Gandin, V., Masvidal, L., Hulea, L., Gravel, S.P., Cargnello, M., McLaughlan, S., Cai, Y.,
868 Balanathan, P., Morita, M., Rajakumar, A., et al. (2016). nanoCAGE reveals 5' UTR
869 features that define specific modes of translation of functionally related MTOR-
870 sensitive mRNAs. Genome Res 26, 636-648.
871 40. Subramanian, A., Tamayo, P., Mootha, V.K., Mukherjee, S., Ebert, B.L., Gillette, M.A.,
872 Paulovich, A., Pomeroy, S.L., Golub, T.R., Lander, E.S., et al. (2005). Gene set
873 enrichment analysis: a knowledge-based approach for interpreting genome-wide
874 expression profiles. Proc Natl Acad Sci U S A 102, 15545-15550.
875 41. Epi, C., Chen, S., Neale, B.M., and Berkovic, S.F. (2023). Shared and distinct ultra-rare
876 genetic risk for diverse epilepsies: A whole-exome sequencing study of 54,423
877 individuals across multiple genetic ancestries. medRxiv.
878 42. Blair, J.D., Hockemeyer, D., and Bateup, H.S. (2018). Genetically engineered human
879 cortical spheroid models of tuberous sclerosis. Nat Med 24, 1568-1578.
880 43. Costa, V., Aigner, S., Vukcevic, M., Sauter, E., Behr, K., Ebeling, M., Dunkley, T., Friedlein,
881 A., Zoffmann, S., Meyer, C.A., et al. (2016). mTORC1 Inhibition Corrects
882 Neurodevelopmental and Synaptic Alterations in a Human Stem Cell Model of
883 Tuberous Sclerosis. Cell Rep 15, 86-95.
884 44. Sundberg, M., Tochitsky, I., Buchholz, D.E., Winden, K., Kujala, V., Kapur, K., Cataltepe,
885 D., Turner, D., Han, M.J., Woolf, C.J., et al. (2018). Purkinje cells derived from TSC

886 patients display hypoexcitability and synaptic deficits associated with reduced FMRP
887 levels and reversed by rapamycin. Mol Psychiatry 23, 2167-2183.
888 45. Zucco, A.J., Pozzo, V.D., Afinogenova, A., Hart, R.P., Devinsky, O., and D'Arcangelo, G.
889 (2018). Neural progenitors derived from Tuberous Sclerosis Complex patients exhibit
890 attenuated PI3K/AKT signaling and delayed neuronal differentiation. Mol Cell Neurosci
891 92, 149-163.
892 46. Dowling, R.J., Topisirovic, I., Alain, T., Bidinosti, M., Fonseca, B.D., Petroulakis, E., Wang,
893 X., Larsson, O., Selvaraj, A., Liu, Y., et al. (2010). mTORC1-mediated cell proliferation,
894 but not cell growth, controlled by the 4E-BPs. Science 328, 1172-1176.
895 47. Oertlin, C., Watt, K., Ristau, J., and Larsson, O. (2022). Anota2seq Analysis for
896 Transcriptome-Wide Studies of mRNA Translation. Methods Mol Biol 2418, 243-268.
897 48. Sandri, B.J., Masvidal, L., Murie, C., Bartish, M., Avdulov, S., Higgins, L., Markowski, T.,
898 Peterson, M., Bergh, J., Yang, P., et al. (2019). Distinct Cancer-Promoting Stromal
899 Gene Expression Depending on Lung Function. Am J Respir Crit Care Med 200, 348-
900 358.
901 49. Bartish, M., Abraham, M.J., Goncalves, C., Larsson, O., Rolny, C., and Del Rincon, S.V.
902 (2023). The role of eIF4F-driven mRNA translation in regulating the tumour
903 microenvironment. Nat Rev Cancer 23, 408-425.
904 50. Tahmasebi, S., Khoutorsky, A., Mathews, M.B., and Sonenberg, N. (2018). Translation
905 deregulation in human disease. Nat Rev Mol Cell Biol 19, 791-807.
906 51. Lee, B.J., Boyer, J.A., Burnett, G.L., Thottumkara, A.P., Tibrewal, N., Wilson, S.L., Hsieh,
907 T., Marquez, A., Lorenzana, E.G., Evans, J.W., et al. (2021). Selective inhibitors of
908 mTORC1 activate 4EBP1 and suppress tumor growth. Nat Chem Biol 17, 1065-1074.
909 52. Silvera, D., Ernlund, A., Arju, R., Connolly, E., Volta, V., Wang, J., and Schneider, R.J.
910 (2017). mTORC1 and -2 Coordinate Transcriptional and Translational Reprogramming
911 in Resistance to DNA Damage and Replicative Stress in Breast Cancer Cells. Mol Cell
912 Biol 37.

913 53. Volta, V., Perez-Baos, S., de la Parra, C., Katsara, O., Ernlund, A., Dornbaum, S., and
914 Schneider, R.J. (2021). A DAP5/eIF3d alternate mRNA translation mechanism
915 promotes differentiation and immune suppression by human regulatory T cells. Nat
916 Commun 12, 6979.
917 54. Mamane, Y., Petroulakis, E., Martineau, Y., Sato, T.A., Larsson, O., Rajasekhar, V.K., and
918 Sonenberg, N. (2007). Epigenetic activation of a subset of mRNAs by eIF4E explains
919 its effects on cell proliferation. PLoS One 2, e242.
920 55. Beggs, J.E., Tian, S., Jones, G.G., Xie, J., Iadevaia, V., Jenei, V., Thomas, G., and Proud,
921 C.G. (2015). The MAP kinase-interacting kinases regulate cell migration, vimentin
922 expression and eIF4E/CYFIP1 binding. Biochem J 467, 63-76.
923 56. Robichaud, N., del Rincon, S.V., Huor, B., Alain, T., Petruccelli, L.A., Hearnden, J.,
924 Goncalves, C., Grotegut, S., Spruck, C.H., Furic, L., et al. (2015). Phosphorylation of
925 eIF4E promotes EMT and metastasis via translational control of SNAIL and MMP-3.
926 Oncogene 34, 2032-2042.
927 57. Liao, C., Moyses-Oliveira, M., De Esch, C.E.F., Bhavsar, R., Nuttle, X., Li, A., Yu, A., Burt,
928 N.D., Erdin, S., Fu, J.M., et al. (2023). Convergent coexpression of autism-associated
929 genes suggests some novel risk genes may not be detectable in large-scale genetic
930 studies. Cell Genom 3, 100277.
931 58. Ascano, M., Jr., Mukherjee, N., Bandaru, P., Miller, J.B., Nusbaum, J.D., Corcoran, D.L.,
932 Langlois, C., Munschauer, M., Dewell, S., Hafner, M., et al. (2012). FMRP targets
933 distinct mRNA sequence elements to regulate protein expression. Nature 492, 382-
934 386.
935 59. Darnell, J.C., Van Driesche, S.J., Zhang, C., Hung, K.Y., Mele, A., Fraser, C.E., Stone,
936 E.F., Chen, C., Fak, J.J., Chi, S.W., et al. (2011). FMRP stalls ribosomal translocation
937 on mRNAs linked to synaptic function and autism. Cell 146, 247-261.

938 60. Das Sharma, S., Metz, J.B., Li, H., Hobson, B.D., Hornstein, N., Sulzer, D., Tang, G., and
939 Sims, P.A. (2019). Widespread Alterations in Translation Elongation in the Brain of
940 Juvenile Fmr1 Knockout Mice. Cell Rep 26, 3313-3322 e3315.
941 61. Flanagan, K., Baradaran-Heravi, A., Yin, Q., Dao Duc, K., Spradling, A.C., and Greenblatt,
942 E.J. (2022). FMRP-dependent production of large dosage-sensitive proteins is highly
943 conserved. Genetics 221.
944 62. Richter, J.D., and Zhao, X. (2021). The molecular biology of FMRP: new insights into
945 fragile X syndrome. Nat Rev Neurosci 22, 209-222.
946 63. Sawicka, K., Hale, C.R., Park, C.Y., Fak, J.J., Gresack, J.E., Van Driesche, S.J., Kang,
947 J.J., Darnell, J.C., and Darnell, R.B. (2019). FMRP has a cell-type-specific role in CA1
948 pyramidal neurons to regulate autism-related transcripts and circadian memory. Elife
949 8.
950 64. Gabriele, M., Lopez Tobon, A., D'Agostino, G., and Testa, G. (2018). The chromatin basis
951 of neurodevelopmental disorders: Rethinking dysfunction along the molecular and
952 temporal axes. Prog Neuropsychopharmacol Biol Psychiatry 84, 306-327.
953 65. Mossink, B., Negwer, M., Schubert, D., and Nadif Kasri, N. (2021). The emerging role of
954 chromatin remodelers in neurodevelopmental disorders: a developmental perspective.
955 Cell Mol Life Sci 78, 2517-2563.
956 66. Guan, B.J., van Hoef, V., Jobava, R., Elroy-Stein, O., Valasek, L.S., Cargnello, M., Gao,
957 X.H., Krokowski, D., Merrick, W.C., Kimball, S.R., et al. (2017). A Unique ISR Program
958 Determines Cellular Responses to Chronic Stress. Mol Cell 68, 885-900 e886.
959 67. Pakos-Zebrucka, K., Koryga, I., Mnich, K., Ljujic, M., Samali, A., and Gorman, A.M. (2016).
960 The integrated stress response. EMBO Rep 17, 1374-1395.
961 68. Klann, K., Tascher, G., and Munch, C. (2020). Functional Translatome Proteomics Reveal
962 Converging and Dose-Dependent Regulation by mTORC1 and eIF2alpha. Mol Cell 77,
963 913-925 e914.

964 69. Sun, E., and Shi, Y. (2015). MicroRNAs: Small molecules with big roles in
965 neurodevelopment and diseases. Exp Neurol 268, 46-53.
966 70. Pawlik, B., Grabia, S., Smyczynska, U., Fendler, W., Drozdz, I., Liszewska, E., Jaworski,
967 J., Kotulska, K., Jozwiak, S., Mlynarski, W., et al. (2022). MicroRNA Expression Profile
968 in TSC Cell Lines and the Impact of mTOR Inhibitor. Int J Mol Sci 23.
969 71. Mor, M., Nardone, S., Sams, D.S., and Elliott, E. (2015). Hypomethylation of miR-142
970 promoter and upregulation of microRNAs that target the oxytocin receptor gene in the
971 autism prefrontal cortex. Mol Autism 6, 46.
972

973 **FIGURE TITLES AND LEGENDS**

974

975 **Figure 1. Treatment with RMC-6272 or rapamycin rescues increased cell size in *TSC2*-**
976 **mutant NPCs.**
977 (A) Schematic representation of how mTORC1 signaling modulates mRNA translation.
978 Inhibitors used to target the pathway axes are indicated in red.
979 (B) Representative bright field images, including enlarged inset images (black boxed regions),
980 are shown for *TSC2*-Het and -Null NPCs compared with *TSC2*-WT cells. Scale bar=100µm.
981 (C) Immunoblotting of an isogenic set of *TSC2*-WT, -Het and -Null (cl. 39) NPCs, following 24
982 h treatment with DMSO (control), rapamycin (50nM) or RMC-6272 (10nM) are shown for
983 TSC2/tuberin as well as mTORC1 pathway readouts pS6K T389, pS6 S240/244 and p4E-BP1
984 S65 along with respective total proteins.
985 (D) Average cell size for *TSC2*-Het and -Null NPCs relative to *TSC2*-WT cells following 48 h
986 with DMSO (control), rapamycin or RMC-6272 (same concentrations as in C) was quantitated,
987 and data represents the mean (±SEM) from 3 independent experiments, each with triplicate
988 technical replicates. P-values of comparisons (*$p<0.05$, **$p<0.01$, ***$p<0.001$) from Students
989 t-test are indicated.
990

991 **Figure 2. Altered neurodevelopmental phenotypes in *TSC2* mutant NPCs are rescued**
992 **by RMC-6272, but not rapamycin.**
993 (A) Proliferation by live cell counting (trypan blue exclusion) was carried out over days D1-4
994 in *TSC2*-WT, -Het and -Null NPCs under control treatment (left graph region), or treatment
995 initiated at D1 with rapamycin (50 nM, middle graph region) or RMC-6272 (10 nM, right graph
996 region). Quantitation for each timepoint is normalized to cell seeding number (D0=1). Data
997 represents the mean (±SEM) from 3 independent experiments (3 replicates/cell
998 line/experiment). Student's t-test p-values (*p<0.05, **p<0.01, ***p<0.001) are indicated in
999 DMSO-treated NPCs (left graph region) for increasing cell numbers in *TSC2*-Het and Null
1000 NPCs at each timepoint (D1-4) relative to *TSC2*-WT NPCs at the respective timepoint. For
1001 drug-treated NPCs (middle and right graph regions), within each genotype, p-values are
1002 indicated for changes in cell numbers relative to DMSO controls at the corresponding
1003 timepoint.
1004 (B) Representative images of immunofluorescence staining in NPCs using neuronal marker
1005 MAP2 (gray), performed 48 h after initiating nerite outgrowth, are shown along with traced
1006 images generated employing HCA-Vision image quantitation software (green), which traces
1007 the cell body along branching layers of the neurite arborization. Scale bar = 100 µm.
1008 (C and D) Bar plots indicate average neurite length (left panel), average neurite number
1009 (center) and extremities (right) per cell for *TSC2*-Het and -Null NPCs relative to *TSC2*-WT
1010 NPCs under control conditions (C) or for rapamycin (50 nM) or RMC-6272 (10 nM) treatment
1011 in *TSC2*-Het and -Null cells relative to DMSO control (D) . Data represents mean (±SEM) from
1012 3 independent experiments (8 non-overlapping image fields/cell line/experiment). P-values
1013 from Student's t-test (*p<0.05, **p<0.01, ***p<0.001) are shown.
1014
1015 **Figure 3. Extensive remodeling of mRNA translation in *TSC2*-Null NPCs aligns with**
1016 **those observed following loss of *TSC1*.**

1017 (A) Scatterplot of polysome-associated mRNA versus total mRNA log2 fold changes between
1018 *TSC2*-Null (-/-) and WT NPCs. Genes are colored according to their mode of regulation as
1019 identified by the anota2seq analysis (FDR < 0.15). The number of mRNAs regulated via
1020 translation, mRNA abundance or offsetting is indicated.
1021 (B) Kernel densities of p-values and FDRs (from anota2seq analysis) for the comparison of
1022 *TSC2*-Null versus WT NPCs. Densities are shown for analysis of polysome-associated RNA
1023 (translated mRNA), total mRNA, translation and offsetting. A shift of the density towards low
1024 p-values/FDRs indicates a higher frequency of changes.
1025 (C) Enrichment of top ten gene ontology annotation for biological processes among genes that
1026 undergo significant changes in translation (light red – activated translation, dark red –
1027 suppressed translation) in *TSC2*-Null versus WT NPCs.
1028 (D) Scatterplots from anota2seq analysis of *TSC2*-Null versus WT NPCs (top left and bottom
1029 right panels) and *TSC1*-Null versus WT NPCs (top right and bottom left panels). Transcripts
1030 identified as regulated by translation in anota2seq analysis in the *TSC2*-Null versus WT NPC
1031 (top left and right panels) or *TSC1*-Null versus WT NPC (bottom left and right panels)
1032 comparisons are indicated. Also shown are empirical cumulative distribution functions of the
1033 log2 fold changes in translation for the corresponding gene sets. Grey dots and lines
1034 correspond to the background (i.e. not in gene sets). Significant shifts of gene sets, relative to
1035 control, were determined using Wilcoxon rank-sum test and the resulting p-values are shown.
1036 (E) Venn diagrams comparing translationally regulated genes identified in anota2seq analysis
1037 following loss of *TSC1* or *TSC2*.
1038 (F) Enrichments of gene ontology annotation for biological processes among genes identified
1039 as showing consistent regulation in both *TSC1*-Null and *TSC2*-Null NPCs relative to their
1040 controls (same color codes as in panel C).
1041
1042 **Figure 4. Suppressed translation of transcripts encoding ASD- and NDD-associated**
1043 **proteins in *TSC2*-Null NPCs associates with distinct 5'UTR features.**

1044 (A) GSEA analysis of ASD- and NDD-associated genes and anota2seq analysis of translation
1045 (fold-changes) of the comparison of *TSC2*-Null (-/-) versus WT NPCs. Rankings for ASD- and
1046 NDD-associated genes (ASD72 and NDD373, respectively) were shifted towards the right
1047 denoting suppressed translation. Normalized enrichment scores (NES) and adjusted p-values
1048 are shown.
1049 (B) Scatterplots from anota2seq analysis for *TSC2*-Null versus WT NPCs. High confidence
1050 ASD- and NDD-associated genes (ASD72 and NDD373, respectively) (top left panel) as well
1051 as eIF4E- (middle left panel) or mTOR-sensitive (bottom left panel) transcripts are indicated.
1052 Shown to the right of each panel are corresponding empirical distribution functions together
1053 with associated statistics (as in Fig. 3D).
1054 (C-D) Boxplots of 5'UTR lengths (C) and GC-contents (D) (according to the RefSeq database,
1055 version 109.20201120) for ASD- and NDD-associated genes as well as mRNAs translationally
1056 regulated in *TSC2*-Null versus WT NPCs (after excluding ASD- and NDD-associated genes;
1057 background corresponds to mRNAs not in any of the subsets). The mean length or GC-
1058 contents for each set are indicated together with p-values from Wilcoxon-tests. (E) The
1059 proportion of mRNAs harboring upstream open reading frames (uORFs) in their 5'UTRs
1060 among subsets of transcripts from C-D. The lower part of the bar graphs corresponds to
1061 uORFs with a strong Kozak context. Differences in proportions of uORFs were assessed using
1062 Fisher's exact tests for the indicated comparisons.
1063
1064 **Figure 5. mTORC1 or MNK1/2 inhibition leads to changes in mRNA translation and**
1065 **reverses translation of suppressed transcripts in *TSC2*-Null NPCs.**
1066 (A and B) Scatterplots from anota2seq analysis of *TSC2*-Null NPCs treated with RMC-6272
1067 versus DMSO (A, top left panel) or eFT-508 versus DMSO (B, top left panel). Transcripts
1068 identified as regulated by translation in anota2seq analysis in the RMC-6272 versus DMSO
1069 treated NPCs (A, left panels) or eFT-508 versus DMSO treated NPCs (B, left panels)
1070 comparisons are indicated. Also shown are empirical cumulative distribution functions (A and

1071 B, right panels) of the log2 fold changes in translation for the corresponding gene sets. Grey
1072 dots and lines correspond to the background (i.e. not in gene sets). Significant shifts of gene
1073 sets, relative to control, were determined using Wilcoxon rank-sum test and the resulting p-
1074 values are shown.
1075 (C) Assessing how transcripts whose translation was altered in *TSC2*-Null vs WT NPCs (top
1076 panel, from Fig. 3A) are modulated upon treatment with RMC-6272 (bottom left panel) or eFT-
1077 508 (bottom right panel).
1078 (D) Enrichments of gene ontology annotation for biological processes among genes identified
1079 as showing reversal in translation overlapping between RMC-6272 and eFT-508 treatment
1080 (same color codes as in Figure 3C).
1081
1082 **Figure 6. mTORC1 or MNK1/2 inhibition reverses translation of suppressed transcripts**
1083 **encoding ASD- and NDD-associated proteins in *TSC2*-Null NPCs.**
1084 (A) Scatterplots for high confidence ASD- and NDD-associated genes (ASD72 and NDD373)
1085 from anota2seq analysis of *TSC2*-Null versus WT NPCs (top panel) as well as RMC-6272
1086 (bottom left) or eFT508 (bottom right) treatment of *TSC2*-Null NPCs are shown. The shape
1087 and position of ellipses correspond to the mean and standard deviation for all genes within
1088 each gene set, respectively.
1089 (B) A Venn diagram comparing ASD associated genes (ASD72) whose translation was
1090 suppressed in *TSC2*-Null NPC relative to *TSC2*-WT NPCs and reversed by treatment with
1091 RMC-6272 or eFT-508.
1092 (C) Plots denote RT-qPCR analysis from the polysome-associated RNA pool (3 biological
1093 replicates) for 5 ASD- or NDD-associated genes (left) as well as 5 eIF4E-sensitive genes
1094 (right) from the indicated cells and treatments. Data were normalized to total mRNA obtained
1095 in parallel as well as beta-actin mRNA expression. P-values from student's t-test test (*$p<0.05$,
1096 **$p<0.01$, ***$p<0.001$) for the indicated comparisons are shown.
1097

| Drug Tx* | Direction of regulation | Geneset name | # Genes | pV | Gene ID |
|---|---|---|---|---|---|
| DMSO | Down (baseline) | ASD72 | 31 | 1.72E-07 | *MED13, NIPBL, ASH1L, KMT2A, CHD2, EHMT1, KMT5B, CHD8, WAC, RFX3, TLK2, SMARCC2, POGZ, KMT2C, ADNP, KCNB1, MEIS2, ASXL3, DYRK1A, SPAST, SETD5, VEZF1, AUTS2, NRXN1, TCF7L2, TAOK1, NF1, ZBTB20, MED23, KDM5B, DNMT3A* |
| RMC | Up | ASD72 | 28 | 1.78E-11 | *MED13, NIPBL, ASH1L, KMT2A, CHD2, EHMT1, KMT5B, CHD8, WAC, RFX3, TLK2, POGZ, KMT2C, ADNP, MEIS2, ASXL3, DYRK1A, SPAST, SETD5, VEZF1, AUTS2, NRXN1, TCF7L2, TAOK1, NF1, MED23, KDM5B, DNMT3A* |
| eFT508 | Up | ASD72 | 18 | 8.63E-06 | *MED13, NIPBL, ASH1L, KMT2A, CHD2, KMT5B, WAC, RFX3, KMT2C, MEIS2, ASXL3, SPAST, VEZF1, AUTS2, NRXN1, TCF7L2, TAOK1, NF1* |
| n/a | Down (baseline) | NDD373 | 138 | 2.59E-19 | *MED13, NIPBL, SMC3, CNOT1, KMT2E, UBTF, KDM3B, TRRAP, USP7, ASH1L, KMT2A, CREBBP, KAT6A, SIN3A, CHD2, ARID1A, SPEN, EHMT1, TLE3, UBR5, CHD7, KMT5B, HIVEP2, CHD8, WAC, ZNF462, NSD1, ARID2, GATAD2B, FBXO11, TAB2, HDAC2, KMT2D, ZNF148, RFX3, TBL1XR1, ZEB2, SETBP1, PHIP, TLK2, RAI1, KIF5C, SMARCC2, SON, STAG1, POGZ, ZMYND11, KIF11, KMT2C, ADNP, KCNB1, COL4A1, KAT6B, SCN8A, ZMYND8, RFX7, PHF12, ZFHX3, SHOC2, TRIO, SOS1, ZNF292, ZFHX4, GNB1, SETD1B, TANC2, KIF2A, ARIH1, SOX9, ACVR2A, TNRC6B, SET, MEIS2, CTNND1, SMARCE1, GLI3, YY1, ASXL3, PDE4D, SETD2, SYNCRIP, BRAF, MAP3K7, DYRK1A, WDR48, TCF4, SRP54, SMAD4, SPAST, SETD5, HNRNPD, PIK3R1, SNAP25, FBXW7, VEZF1, SRSF1, KLF7, TOP2B, ZMIZ1, AUTS2, NRXN1, TRIM8, PPP2CA, CHAMP1, TCF7L2, TAOK1, ATF2, ZBTB10, NF1, SATB1, CSNK2A1, BICD2, CAPRIN1, ZBTB20, CDK13, ZMYM2, GABRB3, CBX5, TCF12, MAP2K1, MYCN, CDK8, SOX11, SYT1, TRPM3, RAC1, MSL2, ABCC9, MED23, DNM1L, KLHL20, TNPO3, KDM5B, KBTBD7, PPM1D, KRAS, DNMT3A, MIB1* |
| RMC | Up | NDD373 | 96 | 4.37E-18 | *MED13, NIPBL, SMC3, CNOT1, KMT2E, UBTF, TRRAP, USP7, ASH1L, KMT2A, CREBBP, KAT6A, SIN3A, CHD2, EHMT1, TLE3, UBR5, CHD7, KMT5B, HIVEP2, CHD8, WAC, ZNF462, NSD1, ARID2, FBXO11, TAB2, KMT2D, ZNF148, RFX3, ZEB2, SETBP1, TLK2, RAI1, KIF5C, SON, STAG1, POGZ, ZMYND11, KIF11, KMT2C, ADNP, COL4A1, KAT6B, SCN8A, ZMYND8, PHF12, ZFHX3, SHOC2, TRIO, SOS1, ZNF292, SETD1B, TANC2, ARIH1, SOX9, ACVR2A, TNRC6B, MEIS2, CTNND1, YY1, ASXL3, PDE4D, SETD2, MAP3K7, DYRK1A, WDR48, SRP54, SPAST, SETD5, PIK3R1, SNAP25, VEZF1, KLF7, ZMIZ1, AUTS2, NRXN1, PPP2CA, CHAMP1, TCF7L2, TAOK1, ZBTB10, NF1, SATB1, CDK13, MAP2K1, MYCN, SYT1, TRPM3, MSL2, ABCC9, MED23, KLHL20, KDM5B, PPM1D, DNMT3A* |
| eFT508 | Up | NDD373 | 69 | 1.48E-10 | *MED13, NIPBL, SMC3, KMT2E, ASH1L, KMT2A, KAT6A, SIN3A, CHD2, SPEN, UBR5, KMT5B, HIVEP2, WAC, ZNF462, ARID2, FBXO11, TAB2, KMT2D, ZNF148, RFX3, ZEB2, KIF5C, STAG1, ZMYND11, KIF11, KMT2C, KAT6B, SCN8A, RFX7, ZFHX3, SHOC2, TRIO, SOS1, ZNF292, TANC2, KIF2A, ARIH1, ACVR2A, MEIS2, ASXL3, PDE4D, SETD2, BRAF, MAP3K7, WDR48, SRP54, SPAST, PIK3R1, SNAP25, VEZF1, ZMIZ1, AUTS2, NRXN1, CHAMP1, TCF7L2, TAOK1, ATF2, ZBTB10, NF1, SATB1, CDK13, GABRB3, SYT1, ABCC9, DNM1L, KLHL20, TNPO3, MIB1* |
| n/a | Down (baseline) | EPI | 22 | 5.82E-03 | *KMT2E, DHX57, TTF1, KDM5B, TTI1, PCDH19, NCOA1, CDKAL1, KANSL1L, DYRK1A, CHD9, ORC2, FAM184A, TUT7, BIRC6, ALKBH8, SETD1B, ANK1, SLC6A16, BPTF, ZSCAN26, PMFBP1* |
| RMC | Up | EPI | 19 | 6.97E-05 | *KMT2E, DHX57, KDM5B, TTI1, PCDH19, NCOA1, KANSL1L, DYRK1A, CHD9, ORC2, FAM184A, TUT7, BIRC6, ALKBH8, SETD1B, SLC6A16, BPTF, ZSCAN26, PMFBP1* |
| eFT508 | Up | EPI | 11 | 3.32E-02 | *KMT2E, PCDH19, NCOA1, CHD9, FAM184A, TUT7, BIRC6, ALKBH8, SLC6A16, BPTF, PMFBP1* |

**Table 1. Gene set enrichment analysis of translationally downregulated genes in *TSC2*-Null NPCs related to ASD, NDD and epilepsy.** *Drug Tx, treatment: DMSO, 10 nM RMC-6272 or 50 nM eFT508; pV, p-value; ASD72, 72 gene variants (false discovery rate (FDR)<0.001) identified in patients with autism spectrum disorder; NDD373, 373 gene variants (FDR<0.001) identified in patients with neurodevelopmental disorders [37]; EPI83, 83 gene variants identified in full epilepsy cohort [41].

# Figure 1

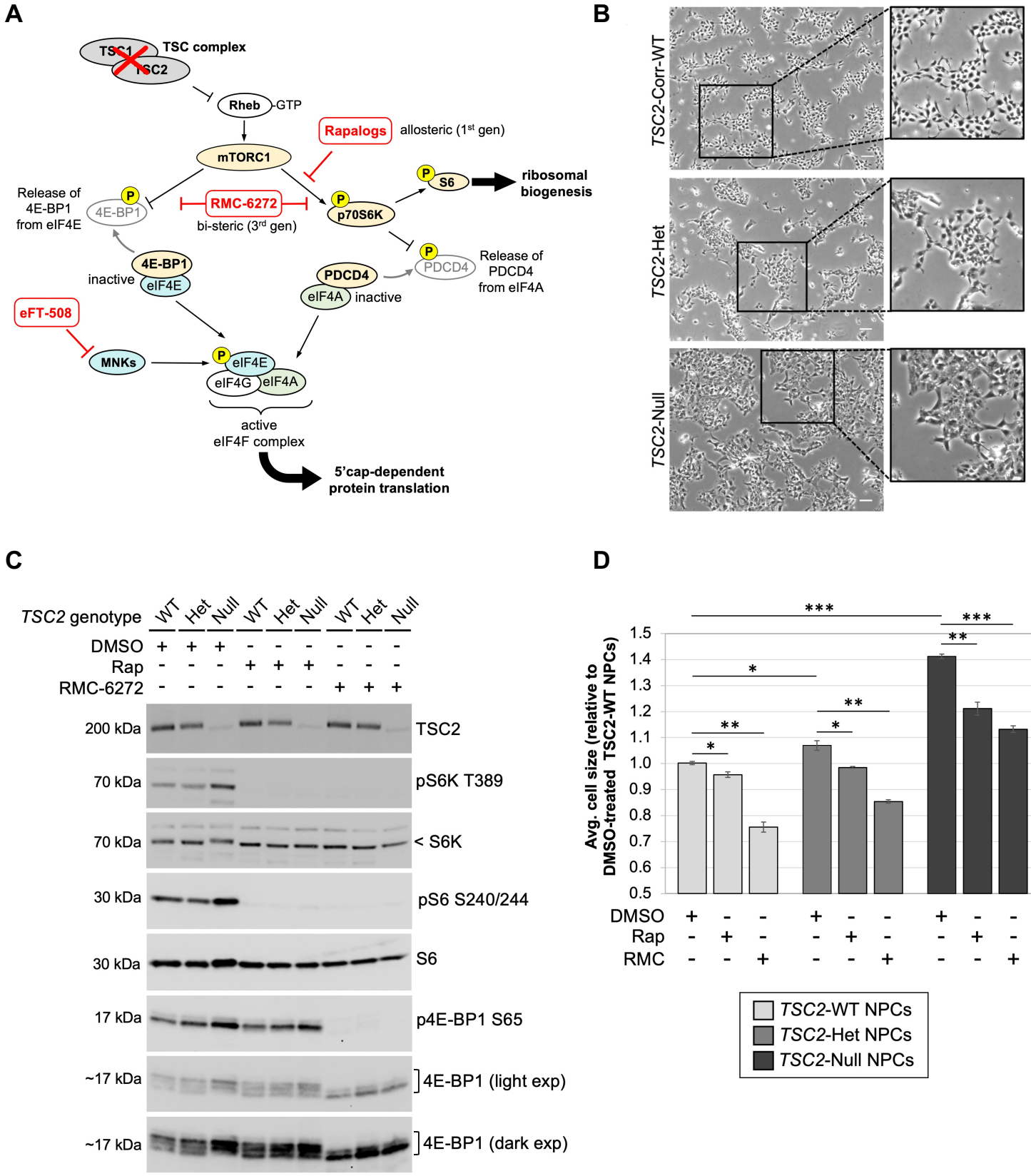
A
TSC complex
TSC1
TSC2
Rheb
GTP
mTORC1
Rapalogs
allosteric (1st gen)
Release of 4E-BP1 from eIF4E
4E-BP1
RMC-6272
bi-steric (3rd gen)
p70S6K
S6
ribosomal biogenesis
4E-BP1
inactive
eIF4E
PDCD4
eIF4A
inactive
PDCD4
Release of PDCD4 from eIF4A
eFT-508
MNKs
eIF4E
eIF4G
eIF4A
active eIF4F complex
5'cap-dependent protein translation
B
TSC2-Corr-WT
TSC2-Het
TSC2-Null
C
TSC2 genotype
WT
Het
Null
DMSO
Rap
RMC-6272
200 kDa
TSC2
70 kDa
pS6K T389
70 kDa
< S6K
30 kDa
pS6 S240/244
30 kDa
S6
17 kDa
p4E-BP1 S65
~17 kDa
4E-BP1 (light exp)
~17 kDa
4E-BP1 (dark exp)
D
Avg. cell size (relative to DMSO-treated TSC2-WT NPCs)
DMSO
Rap
RMC
TSC2-WT NPCs
TSC2-Het NPCs
TSC2-Null NPCs

Figure 2

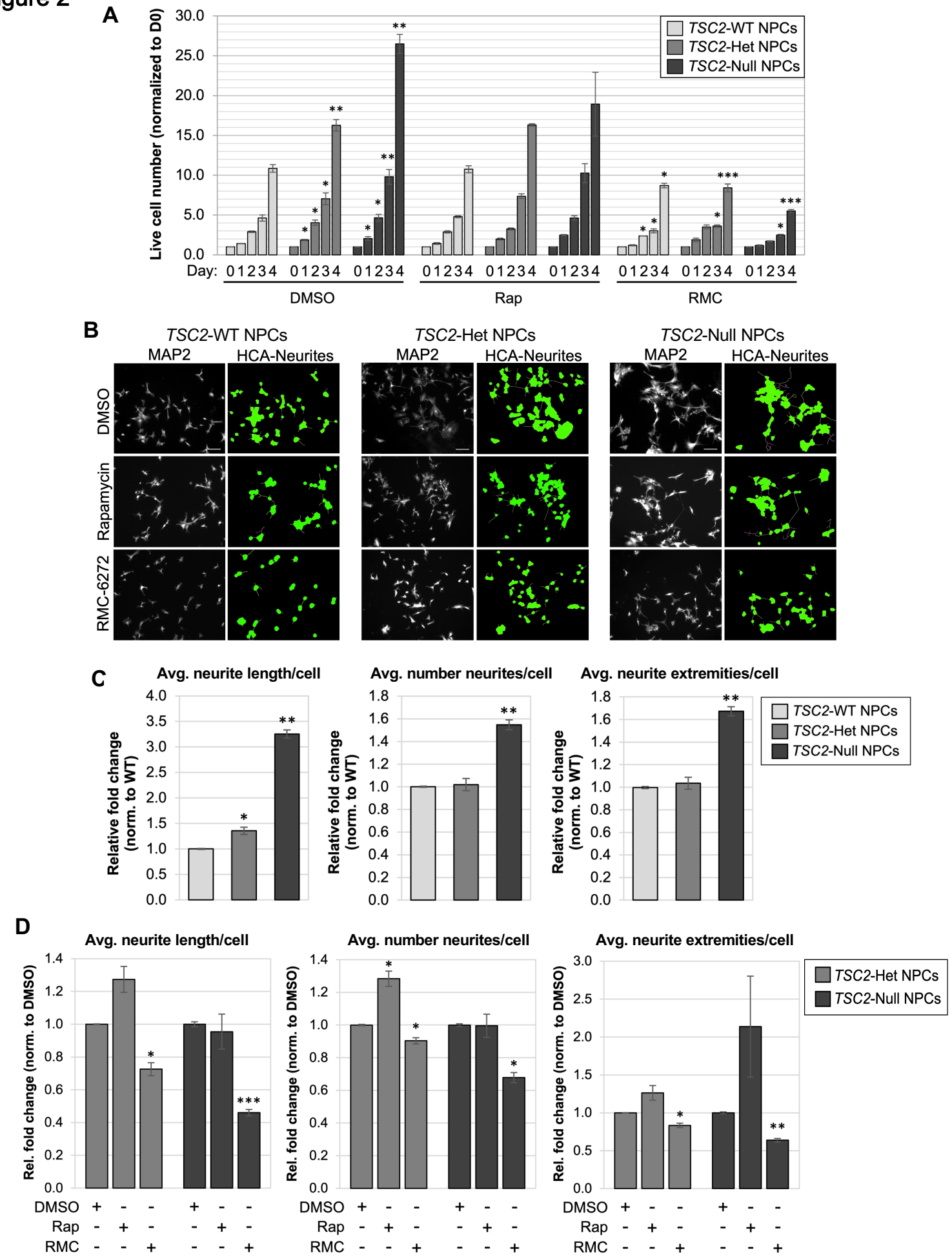
A
Live cell number (normalized to D0)
30.0
25.0
20.0
15.0
10.0
5.0
0.0
TSC2-WT NPCs
TSC2-Het NPCs
TSC2-Null NPCs
Day: 0 1 2 3 4 0 1 2 3 4 0 1 2 3 4 0 1 2 3 4 0 1 2 3 4 0 1 2 3 4 0 1 2 3 4 0 1 2 3 4
DMSO
Rap
RMC
B
TSC2-WT NPCs
TSC2-Het NPCs
TSC2-Null NPCs
MAP2
HCA-Neurites
DMSO
Rapamycin
RMC-6272
C
Avg. neurite length/cell
Avg. number neurites/cell
Avg. neurite extremities/cell
Relative fold change (norm. to WT)
TSC2-WT NPCs
TSC2-Het NPCs
TSC2-Null NPCs
D
Avg. neurite length/cell
Avg. number neurites/cell
Avg. neurite extremities/cell
Rel. fold change (norm. to DMSO)
TSC2-Het NPCs
TSC2-Null NPCs
DMSO
Rap
RMC

# Figure 3

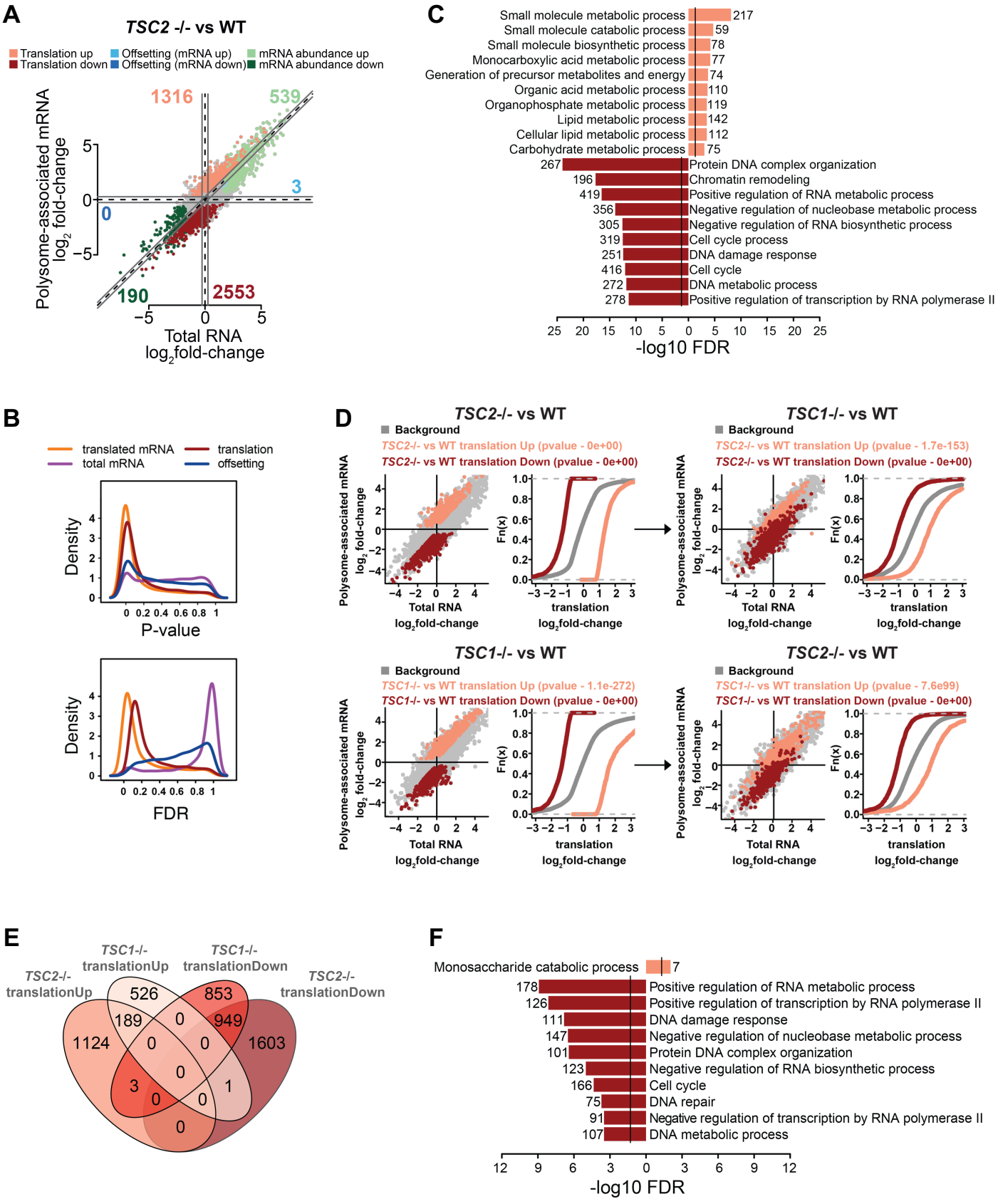
A
TSC2 -/- vs WT
Translation up
Translation down
Offsetting (mRNA up)
Offsetting (mRNA down)
mRNA abundance up
mRNA abundance down
1316
539
3
0
190
2553
Polysome-associated mRNA log2 fold-change
Total RNA log2fold-change
C
Small molecule metabolic process 217
Small molecule catabolic process 59
Small molecule biosynthetic process 78
Monocarboxylic acid metabolic process 77
Generation of precursor metabolites and energy 74
Organic acid metabolic process 110
Organophosphate metabolic process 119
Lipid metabolic process 142
Cellular lipid metabolic process 112
Carbohydrate metabolic process 75
267 Protein DNA complex organization
196 Chromatin remodeling
419 Positive regulation of RNA metabolic process
356 Negative regulation of nucleobase metabolic process
305 Negative regulation of RNA biosynthetic process
319 Cell cycle process
251 DNA damage response
416 Cell cycle
272 DNA metabolic process
278 Positive regulation of transcription by RNA polymerase II
-log10 FDR
B
translated mRNA
total mRNA
translation
offsetting
Density
P-value
FDR
D
TSC2-/- vs WT
Background
TSC2-/- vs WT translation Up (pvalue - 0e+00)
TSC2-/- vs WT translation Down (pvalue - 0e+00)
TSC1-/- vs WT
Background
TSC2-/- vs WT translation Up (pvalue - 1.7e-153)
TSC2-/- vs WT translation Down (pvalue - 0e+00)
TSC1-/- vs WT
Background
TSC1-/- vs WT translation Up (pvalue - 1.1e-272)
TSC1-/- vs WT translation Down (pvalue - 0e+00)
TSC2-/- vs WT
Background
TSC1-/- vs WT translation Up (pvalue - 7.6e99)
TSC1-/- vs WT translation Down (pvalue - 0e+00)
Polysome-associated mRNA log2 fold-change
Total RNA log2fold-change
Fn(x)
translation log2fold-change
E
TSC2-/- translationUp
TSC1-/- translationUp
TSC1-/- translationDown
TSC2-/- translationDown
526
853
189
949
1124
1603
F
Monosaccharide catabolic process 7
178 Positive regulation of RNA metabolic process
126 Positive regulation of transcription by RNA polymerase II
111 DNA damage response
147 Negative regulation of nucleobase metabolic process
101 Protein DNA complex organization
123 Negative regulation of RNA biosynthetic process
166 Cell cycle
75 DNA repair
91 Negative regulation of transcription by RNA polymerase II
107 DNA metabolic process
-log10 FDR

# Figure 4

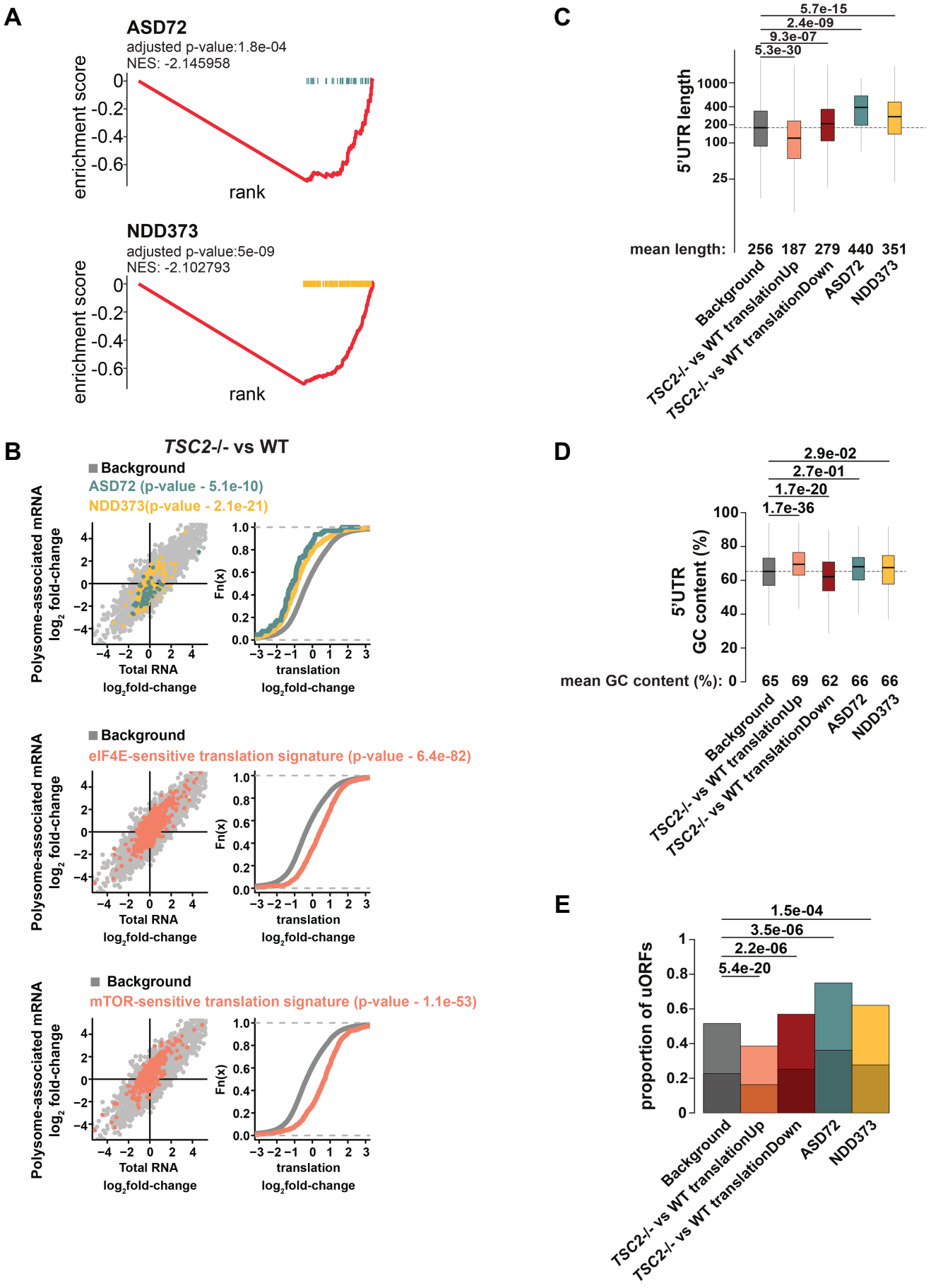
A
ASD72
adjusted p-value:1.8e-04
NES: -2.145958
enrichment score
rank
NDD373
adjusted p-value:5e-09
NES: -2.102793
enrichment score
rank
B
TSC2-/- vs WT
Background
ASD72 (p-value - 5.1e-10)
NDD373(p-value - 2.1e-21)
Polysome-associated mRNA log2 fold-change
Total RNA log2fold-change
Fn(x)
translation log2fold-change
Background
eIF4E-sensitive translation signature (p-value - 6.4e-82)
Background
mTOR-sensitive translation signature (p-value - 1.1e-53)
C
5.7e-15
2.4e-09
9.3e-07
5.3e-30
5'UTR length
mean length: 256 187 279 440 351
Background
TSC2-/- vs WT translationUp
TSC2-/- vs WT translationDown
ASD72
NDD373
D
2.9e-02
2.7e-01
1.7e-20
1.7e-36
5'UTR GC content (%)
mean GC content (%): 65 69 62 66 66
Background
TSC2-/- vs WT translationUp
TSC2-/- vs WT translationDown
ASD72
NDD373
E
1.5e-04
3.5e-06
2.2e-06
5.4e-20
proportion of uORFs
Background
TSC2-/- vs WT translationUp
TSC2-/- vs WT translationDown
ASD72
NDD373

# Figure 5

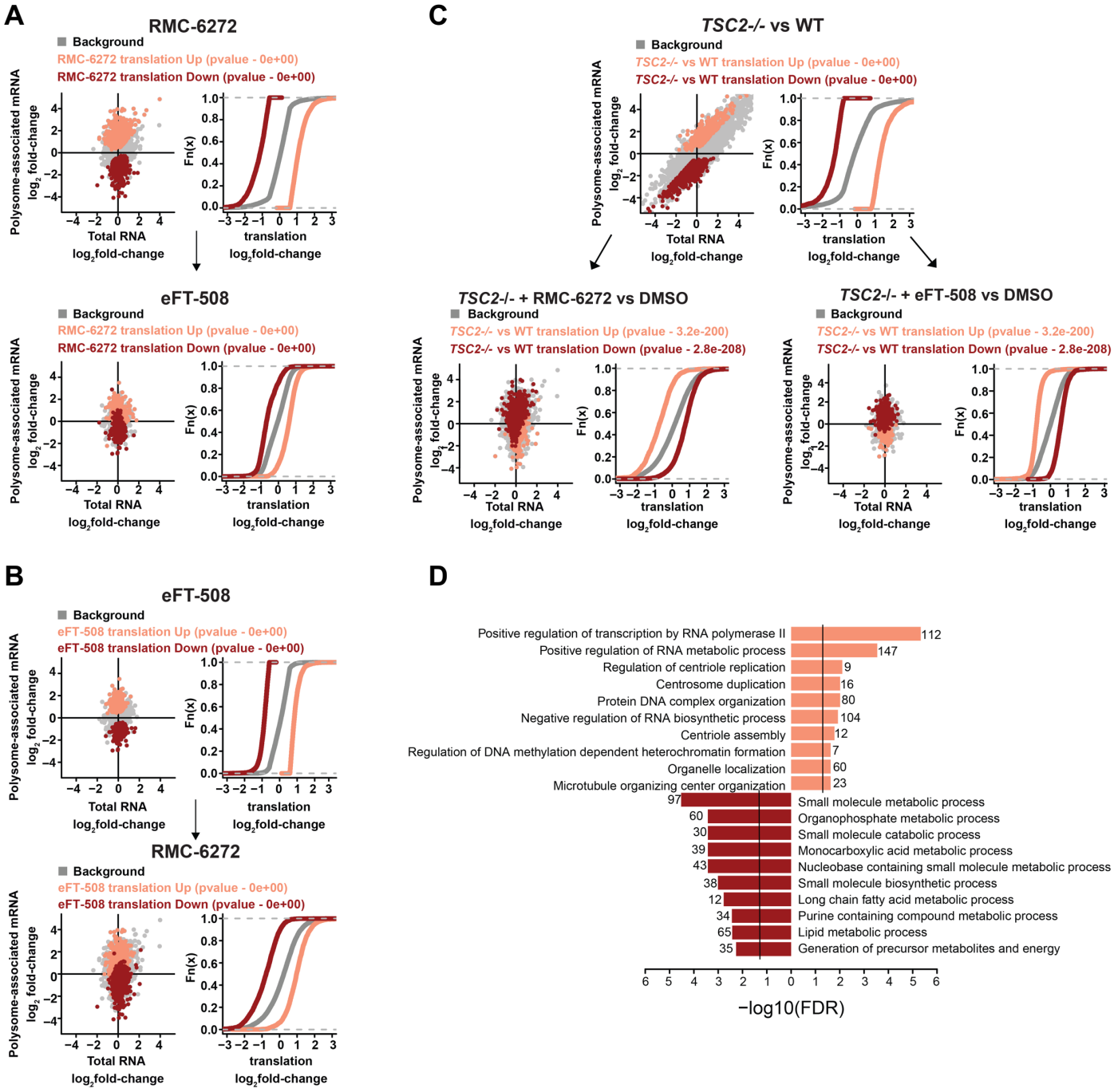
A
RMC-6272
Background
RMC-6272 translation Up (pvalue - 0e+00)
RMC-6272 translation Down (pvalue - 0e+00)
Polysome-associated mRNA log2 fold-change
Total RNA log2fold-change
Fn(x)
translation log2fold-change
eFT-508
Background
RMC-6272 translation Up (pvalue - 0e+00)
RMC-6272 translation Down (pvalue - 0e+00)
B
eFT-508
Background
eFT-508 translation Up (pvalue - 0e+00)
eFT-508 translation Down (pvalue - 0e+00)
RMC-6272
Background
eFT-508 translation Up (pvalue - 0e+00)
eFT-508 translation Down (pvalue - 0e+00)
C
TSC2-/- vs WT
Background
TSC2-/- vs WT translation Up (pvalue - 0e+00)
TSC2-/- vs WT translation Down (pvalue - 0e+00)
TSC2-/- + RMC-6272 vs DMSO
Background
TSC2-/- vs WT translation Up (pvalue - 3.2e-200)
TSC2-/- vs WT translation Down (pvalue - 2.8e-208)
TSC2-/- + eFT-508 vs DMSO
Background
TSC2-/- vs WT translation Up (pvalue - 3.2e-200)
TSC2-/- vs WT translation Down (pvalue - 2.8e-208)
D
Positive regulation of transcription by RNA polymerase II 112
Positive regulation of RNA metabolic process 147
Regulation of centriole replication 9
Centrosome duplication 16
Protein DNA complex organization 80
Negative regulation of RNA biosynthetic process 104
Centriole assembly 12
Regulation of DNA methylation dependent heterochromatin formation 7
Organelle localization 60
Microtubule organizing center organization 23
97 Small molecule metabolic process
60 Organophosphate metabolic process
30 Small molecule catabolic process
39 Monocarboxylic acid metabolic process
43 Nucleobase containing small molecule metabolic process
38 Small molecule biosynthetic process
12 Long chain fatty acid metabolic process
34 Purine containing compound metabolic process
65 Lipid metabolic process
35 Generation of precursor metabolites and energy
−log10(FDR)

# Figure 6

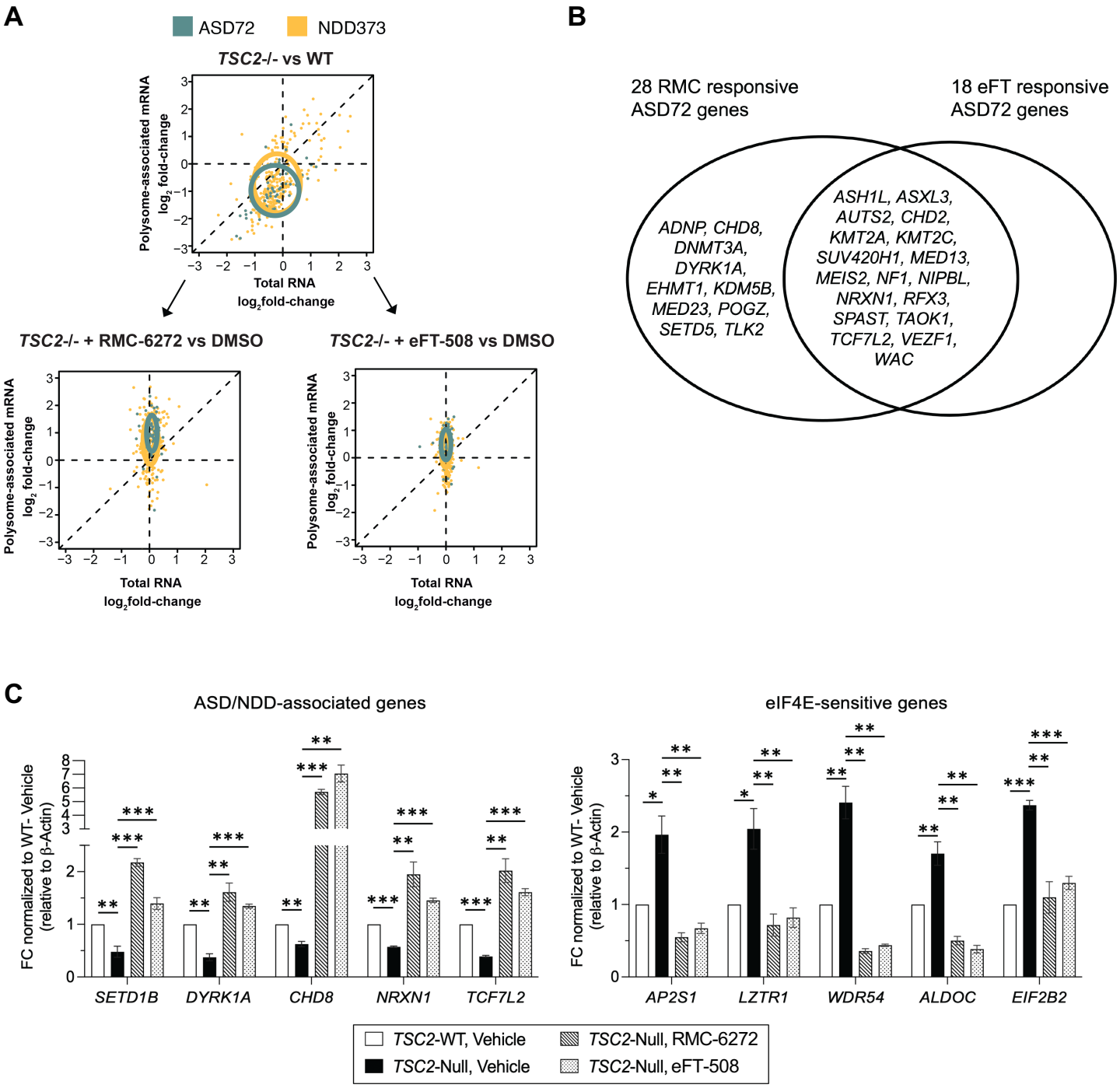
A
ASD72
NDD373
TSC2-/- vs WT
Polysome-associated mRNA log2 fold-change
Total RNA log2fold-change
TSC2-/- + RMC-6272 vs DMSO
TSC2-/- + eFT-508 vs DMSO
B
28 RMC responsive ASD72 genes
18 eFT responsive ASD72 genes
ADNP, CHD8, DNMT3A, DYRK1A, EHMT1, KDM5B, MED23, POGZ, SETD5, TLK2
ASH1L, ASXL3, AUTS2, CHD2, KMT2A, KMT2C, SUV420H1, MED13, MEIS2, NF1, NIPBL, NRXN1, RFX3, SPAST, TAOK1, TCF7L2, VEZF1, WAC
C
ASD/NDD-associated genes
eIF4E-sensitive genes
FC normalized to WT- Vehicle (relative to β-Actin)
SETD1B
DYRK1A
CHD8
NRXN1
TCF7L2
AP2S1
LZTR1
WDR54
ALDOC
EIF2B2
TSC2-WT, Vehicle
TSC2-Null, Vehicle
TSC2-Null, RMC-6272
TSC2-Null, eFT-508